NAVAL POSTGRADUATE SCHOOL
Monterey, California

THESIS

EVALUATION OF THE MECHANICAL PROPERTIES AND EFFECTIVENESS OF COUNTERMINE BOOTS.

by

Richard C. Muschek

March 1998

Thesis Advisor: Young W. Kwon

REPORT DOCUMENTATION PAGE

Form Approved
OMB No. 0704-0188

1. AGENCY USE ONLY	2. REPORT DATE	3. REPORT TYPE AND DATES COVERED
	March 1998	Master's Thesis

4. TITLE AND SUBTITLE
Evaluation of the Mechanical Properties and Effectiveness of Countermine Boots

5. FUNDING NUMBERS

6. AUTHOR(S)
Muschek, Richard C.

7. PERFORMING ORGANIZATION NAME AND ADDRESS
Naval Postgraduate School
Monterey, CA, 93943

8. PERFORMING ORGANIZATION REPORT NUMBER

9. SPONSORING/MONITORING AGENCY NAME AND ADDRESS

10. SPONSORING/MONITORING AGENCY REPORT NUMBER

11. SUPPLEMENTARY NOTES
The views expressed in this report are those of the authors and do not reflect the official policy or position of the Department of Defense or the U.S. Government

12a. DISTRIBUTION/AVAILABILITY STATEMENT
Approved for public release; distribution is unlimited

12b. DISTRIBUTION CODE

12. ABSTRACT(*Maximum of 200 words*)

The first goal of this project was to determine the mechanical properties of countermine boots and protective overboots that are currently available to U.S. soldiers. The second goal of this project was to conduct a qualitative analysis to determine the effectiveness of the boots. This was done by determining their ability to dissipate a blast force equivalent to a typical anti-personnel landmine. This was followed by a parametric study which involved altering the component materials in an effort to determine if the effectiveness of the boots varied as the materials changed.

The soles of both boots were made from identical materials. All the materials used in the boots' soles were tested to determine their mechanical material properties using an Instron uniaxial testing machine. All testing was conducted on multiple specimens to verify repeatability. The material data was tabulated and the stress-strain curves are included in this report.

A finite element analysis was conducted to evaluate the effectiveness of the countermine boot based upon accepted tolerance levels of the lower bones of the body. Next, the materials and their dimensions were modified in the finite element model to determine how these modifications would impact the boots' effectiveness.

14. SUBJECT TERMS	15. NUMBER OF PAGES
Finite Element Method, Material Properties, Mechanical Testing	112
	16. PRICE CODE

17. SECURITY CLASSIFICATION OF REPORT	18. SECURITY CLASSIFICATION OF THIS PAGE	19. SECURITY CLASSIFICATION OF ABSTRACT	20. LIMITATION OF ABSTRACT
Unclassified	Unclassified	Unclassified	UL

NSN 7540-01-280-5500

Standard Form 298 (Rev2-89)
Prescribed by ANSI Std 239-18

EVALUATION OF THE MECHANICAL PROPERTIES AND EFFECTIVENESS OF COUNTERMINE BOOTS

Richard C. Muschek
Captain, United States Army
B.S., United States Military Academy, 1987

Submitted in partial fulfillment of the
requirements for the degree of

MASTER OF SCIENCE IN MECHANICAL ENGINEERING

from the

NAVAL POSTGRADUATE SCHOOL
March, 1998

ABSTRACT

The first goal of this project was to determine the mechanical properties of countermine boots and protective overboots that are currently available to U.S. soldiers. The second goal of this project was to conduct a qualitative analysis to determine the effectiveness of the boots. This was done by determining their ability to dissipate a blast force equivalent to a typical anti-personnel landmine. This was followed by a parametric study which involved altering the component materials in an effort to determine if the effectiveness of the boots varied as the materials changed.

The soles of both boots were made from identical materials. All the materials used in the boots' soles were tested to determine their mechanical material properties using an Instron uniaxial testing machine. All testing was conducted on multiple specimens to verify repeatability. The material data was tabulated and the stress-strain curves are included in this report.

A finite element analysis was conducted to evaluate the effectiveness of the countermine boot based upon accepted tolerance levels of the lower bones of the body. Next, the materials and their dimensions were modified in

the finite element model to determine how these modifications would impact the boots' effectiveness.

TABLE OF CONTENTS

ACKNOWLEDGEMENTS

I would like to sincerely thank Dr. Young W. Kwon for his expertise and guidance with this project. I am very grateful for the assistance of LT Quinten King who unselfishly shared so much of his work and effort.

I dedicate this work to my wife, Marie, and my children, Christopher and Amelia, whose love, support, and many sacrifices contributed to my success in this research.

I. INTRODUCTION AND BACKGROUND

During World War I, the emergence of the main battle tank spurred the development of the Anti-Tank (AT) mine. These first AT mines were clumsy and ill-conceived, being easily redeployed by opposing forces. Between World Wars, a tremendous effort was mounted to develop the Anti-Personnel (AP) mine in order to prevent access these AT mines. Leading military strategists, in particular those in Eastern Europe, began to see ways to expand the AP mine's role in conventional warfare. This was accomplished by linking the mine to the protection of specific military targets and aiming them at enemy soldiers.

After World War II, mines grew not only in popularity but also in sophistication. Hundreds of different types and variations sprang up making detection and disposal significantly more difficult. During the 1960's, a new dangerous application for land mines began to advance. During a nine year bombing campaign of Laos, thousands of mines were air-dropped indiscriminately in an attempt to close the Ho Chi Minh trail. This trend continued during Cambodia's civil war. Opposing factions scattered even more mines randomly throughout the country. Neither side involved in the conflict kept records of where or how many mines were deployed. By the end of the war, more people were killed by AP Mines than by any other armament [Ref. 1].

When the Soviets invaded Afghanistan in 1979, randomly targeted and remotely deployed minefields became a viable and accepted tactic in military doctrine. Cheap, easy to produce, and easy to deploy, land mines became an economical force equalizer for many third world countries. Forces attempting to breech minefields lose not only speed and mobility on the battlefield, but also must expend critical assets to clear maneuver lanes.

Mines also create a psychological advantage. Opposing forces become much more pensive and cautious before advancing when the threat of landmines exists. The fact that AP Mines tend to maim and injure soldiers rather than kill creates a significant strain on the logistical and medical capabilities of an advancing force.

Today an estimated 110 million AP mines are thought to be deployed around the world with another 100 million existing in stock-piles ready for use. With an additional five to ten million being produced annually, AP Mines will continue to remain a significant threat to military personnel and the civilian community well into the future.

The US-made M-14 AP Mine is a typical AP mine in explosive charge and weight. Its design has been copied and used in many other countries as well [Ref. 2]. This study will use this mine as a standard threat while determining the effectiveness of countermine boot.

II. CLASSIFICATION OF AP MINES

To fully appreciate the requirements needed for protective footwear, we must first understand the nature AP Mines. AP Mines are generally classified into two main groups: Blast Mines and Fragmentation Mines. Fragmentation mines are designed to project shrapnel toward the legs and torso of approaching soldiers. Footwear is generally not designed to provide protection against this type of threat. Blast mines are designed to cause injury by subjecting the lower extremities to blast waves. The detonation creates large over pressures and impulses that are transmitted axially to the lower extremities. It is believed that proper engineering design of footwear can significantly reduce the damage inflicted by this type of mine by dissipating this blast wave.

The M-14 AP mine was originally developed in the United States and has been produced under license in the US, India, and Vietnam [Ref. 2]. Several other countries produce similar types of AP mines throughout the world. It has a simple pressure switch actuator requiring approximately 20 pounds of weight to initiate. Its plastic body and small size makes detection difficult even in the best of conditions. The only metal in this mine is a small steel striker tip. This can make it difficult to detect with metal detectors since these detectors are only effective at detecting the metal in the mines. Additionally, the M-14

mine utilizes a main explosive charge of 1 ounce of Tetryl (equivalent to 1.07 ounces of TNT).

III. EXPLOSIVE CHARACTERISTICS OF AP MINES

When an explosive mine is detonated, it creates a hemispherical blast wave. This blast wave is generated when the atmosphere surrounding the explosion is forcibly pushed back by the gases produced from the chemical reaction of the explosive [Ref. 3]. This wave can be illustrated in Figure 3.1. This overpressure can be calculated using Equations 3.1 and 3.2 [Ref. 3]:

$$\frac{p_o}{p} = \frac{808 * \left[1 + \left(\frac{Z}{4.5}\right)^2\right]}{\sqrt{1 + \left(\frac{Z}{0.048}\right)^2} * \sqrt{1 + \left(\frac{Z}{0.32}\right)^2} * \sqrt{1 + \left(\frac{Z}{1.35}\right)^2}} \qquad (3.1)$$

where

$$Z = \frac{d * f_d^{\frac{1}{3}}}{W^{\frac{1}{3}}} \qquad (3.2)$$

The left hand side term of Equation 3.1 is the ratio of the explosion over-pressure to the ambient atmospheric pressure and Z is a scaled distance from the detonation point. In Equation 3.2, d is the distance from the blast in meters, f_d is the transmission factor of atmoshperic density, and W is the scaled weight of the explosive. All constants are calculated for metric units.

Scaling values are used to help make comparisons between similar events. These scaling relations are derived from the same Buckingham PI Theorem that helps engineers

build a scaled model and use it to predict behavior of a full-size plane or other object. In the present case, the scaled distance relates the actual distance, atmospheric density, and the energy released from the chemical reaction of the explosive.

The cubed root values are derived from the geometrical similarity based on a spherical blast. Due to the relatively small amounts of explosives and distances involved, it may be assumed the atmospheric density is homogeneous and uniform throughout the area of interest.

Also of importance is determining the duration of the blast. The amount of energy dissipated over time gives a good indication of the damage causing potential of the blast. A fixed amount of energy dissipated over a longer time will cause less damage than that same amount dissipated quickly. The duration of the blast is considered to be the length of time for which the positive pressure wave exists. For a chemical explosion, this can be calculated using Equation 3.3 [Ref 3]:

$$\frac{T_d}{W^{\frac{1}{3}}} = \frac{980 * \left[1 + \left(\frac{Z}{0.54}\right)^{10}\right]}{\left[1 + \left(\frac{Z}{0.02}\right)^{3}\right] * \left[1 + \left(\frac{Z}{0.74}\right)^{6}\right] * \sqrt{1 + \left(\frac{Z}{6.9}\right)^{2}}} \qquad (3.3)$$

where $t_d/W^{1/3}$ is the duration in milliseconds for a one kilogram TNT explosion in standard atmospheric pressure. Z is the scaled distance as defined above.

For small yield explosions of short duration like those encountered in the case of AP mines, the impulse delivered by the blast is often the leading contributor to the damage-causing ability of the explosion. Impulse can best be visualized as the area under the pressure-time curve. As with the duration of the blast, the significant portion of the impulse is contained under the positive pressure phase of the blast. This portion is then indicative of the entire impulse characteristic of the entire blast wave. The impulse per unit area can be calculated using Equation 3.4 [Ref. 3].

$$\frac{I}{A} = \frac{0.067 * \sqrt{1 + \left(\frac{Z}{0.23}\right)^4}}{Z^2 * \left[1 + \left(\frac{Z}{1.55}\right)^3\right]^{\frac{1}{3}}} \qquad (3.4)$$

Blast wave impulse depends not only on the peak overpressure and the wave duration, but also on the rate of decay of the overpressure. The slower the decay, the greater the area under the curve, thus the greater the impulse provided. This can best be seen in Figure 3.2. This figure shows how the blast wave from a typical nuclear explosion (curve A) decays faster and shows a smaller impulse per unit area than one from a chemical explosion (curve B) with equal initial pressures even though their durations and peak overpressures are identical. (In

reality, typical peak overpressures for nuclear explosions are significantly higher than those associated with chemical explosions.)

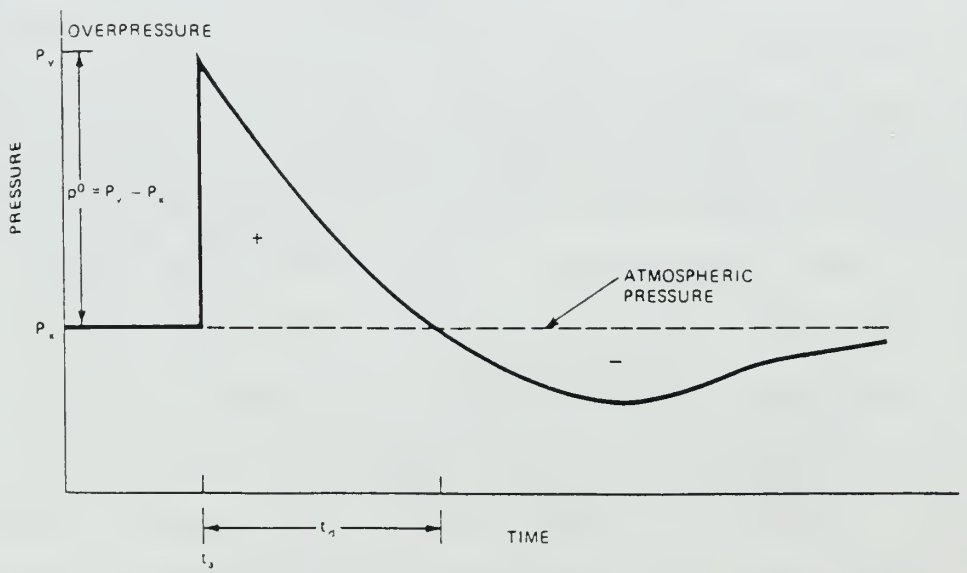

Figure 3.1 Pressure vs time curve for a typical blast wave. From Ref. [3]

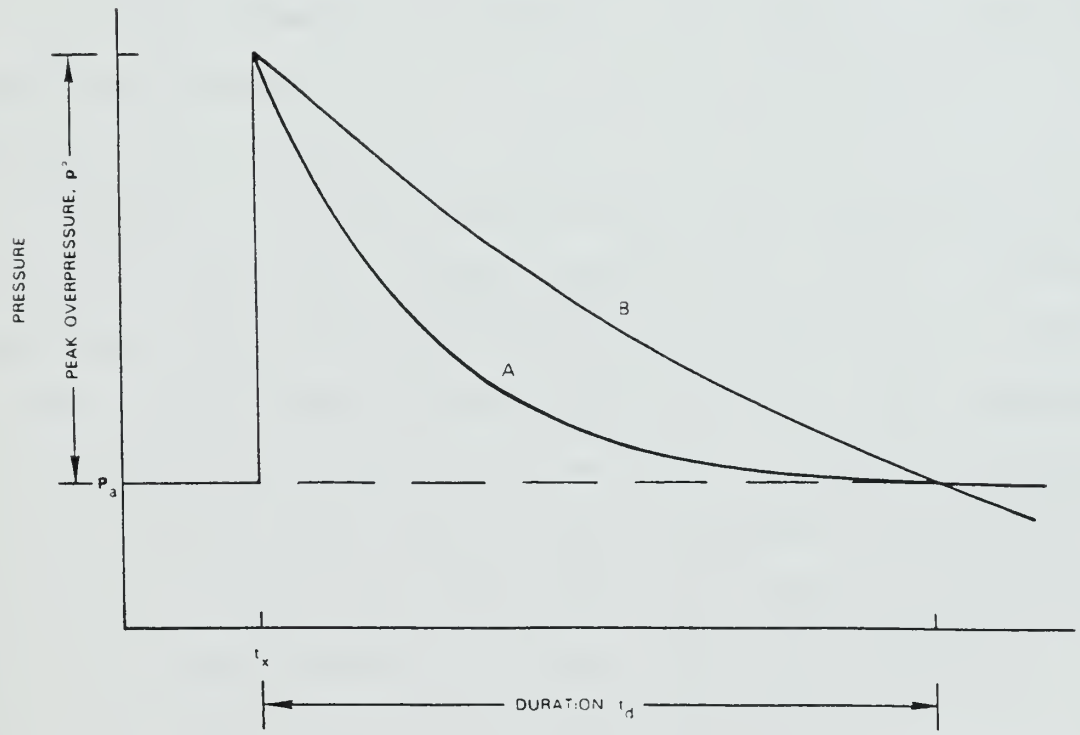

Figure 3.2 Pressure vs time curve comparison. Curve A is a typical nuclear explosion and curve B is a typical chemical explosion. From Ref. [3]

IV. RESEARCH GOAL

The goal of this research is to determine the mechanical properties of countermine boots and protective overboots. The project will then conduct a qualitative analysis to determine the effectiveness of the boots. This will be followed by a parametric study that will involve changing the material types and thickness in an effort to find how the effectiveness of the boots varies as the materials and thickness are changed.

In order to achieve this goal, test specimens were prepared from the already manufactured boots. Because specimens came from manufactured boots and not in sample blocks, there were some limitations in the specimen geometries as well as in the testing. An Instron uniaxial testing machine was used for the mechanical testing and a Scanning Electron Microscopy (SEM) was used in conjunction with a Energy-Dispersive X-Ray (EDX) to determine the chemical compositions of the steel material.

Once the material properties are determined, these properties will be used in a finite element model for simulation of the boot's response to a blast overpressure equivalent to that of an M-14 AP mine. An analysis of the boot's response will determine whether or not the current boot provides sufficient protection for soldiers against such a blast.

Next, variations of the material properties and material dimensions in the finite element model will be analyzed. This will be done to determine trends that may lead to an optimization of the current design of the boot simply by using alternate materials and/or current materials with different dimensions.

Because of a limited budget and scope during this project, a live fire testing of the boots with cadaver limbs could not be performed to verify any of the final results. Data from a live fire testing at the U.S. Army's Aberdeen Proving Ground enabled the verification of the model's response to an equivalent blast. However, in the future, live fire testing involving cadaver limbs should be conducted to verify the model's accuracy involving the lower extremities of the body.

V. SPECIMEN PREPARATION AND TEST PROCEDURE

As mentioned previously, the amount of material to be used as a test specimen was limited in both quantity and shape to that used in each boot. The American Society of Testing Materials (ASTM) [Ref. 4] publishes accepted standards for testing all involved materials in different ways to get different properties. The ASTM standards for specimen dimensions were adhered to as much as possible for the available material. Wherever dimensions and/or test procedures vary from the ASTM is addressed below.

A. RUBBER PREPARATION AND TEST PROCEDURE

1. Specimen Preparation

Due to the available shape of the rubber to be tested (the sole of a boot), testing the rubber in tension was not an option because the bar shaped test specimen required in the ASTM needs more rubber than was available. (See ASTM D412-92 specifications for recommended bar dimensions [Ref. 5].) In addition, shaping the specimen from a rubber already in its final form requires extensive tooling in a machine shop. It was recognized that cutting rubber specimens to precision was difficult [Ref. 6]. Also, the common applications of the rubber used in the sole of a boot are more compressive in nature. Therefore, it was decided

to gather properties for the rubber via compressive tests. ASTM D575-91, Standard Test Methods for Rubber Properties in Compression [Ref. 7], specifies the dimensions of test specimens as 1.129 in in diameter and 0.49 inch in thickness. Given the available contour and thickness of the boot sole, it was obvious that these dimensions were not possible. Therefore, it was determined to use the same ratio of diameter to thickness, 2.3 to 1.0, with smaller sized test specimens. The proper specimen size was 0.39 inch diameter and 0.17 inch thick. (See Figure 5.1) These specimens were milled out using a die fabricated in a machine shop to duplicate recommendations of ASTM D575. The die was placed in a drill press and lubricated with soapy water so that a smooth cut could be obtained. The cutting pressure was kept sufficiently low to avoid "cupping" of the cut surface. The specimens were then cut to the appropriate thickness using a very sharp bladed apparatus used in the construction of delicate models.

2. Test Procedure

The test procedure for the rubber specimens involved applying a constant crosshead speed as a compressive force compresses the cylindrically-shaped specimens. In accordance with ASTM D575, after measuring the exact dimensions of the specimen, each specimen was placed between the crossheads of the testing machine. Sheets of 400 Grit waterproof

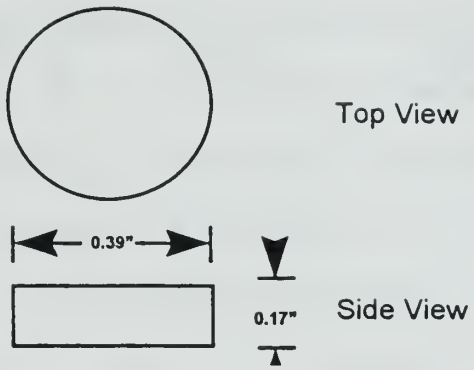

Figure 5.1 Diagram of rubber specimen.

sandpaper were placed between the specimens and the machine surface to resist lateral slippage. (This Grit of sandpaper is also recommended by the ASTM D575.) In accordance with ASTM D575, a continual force was applied at a rate of 0.5 in/min until the desired deflection was achieved. For these tests, compression was continued until the grips of the machine nearly contacted one another. This test procedure was repeated for three different rubber specimens from two separate boots for a total of six specimens.

The Instron machine automatically recorded and stored the load and deflection data that was then downloaded as an ASCII file. This data was then transferred to a MATLAB program. The use of MATLAB eased the manipulation of the raw data for the calculation of strength values, Young's moduli of elasticity, etc, and plotting. This transfer of data via an ASCII file to MATLAB was followed for the data collected for all the test materials.

B. ALUMINUM HONEYCOMB PREPARATION AND TEST PROCEDURE

1. Specimen Preparation

The honeycomb specimen dimensions were also limited by the shape and amount of honeycomb available in each shank. Since testing of the honeycomb was to be conducted to determine the properties in three directions[1], it was desirable to have the shape of all specimens as uniform as possible. A rectangular prism specimen allowed for maximum use of available raw material. Given the shape of the shank, it was determined that 0.9 in x 0.9 in x 0.5 in specimens would optimize the available material for test specimens. (See Figure 5.2) These shapes were cut on a saw in a machine shop at a very slow rate and with minimal clamping pressure. It was found that application of too much clamping pressure on the honeycomb caused the bonding between the aluminum sheets toseparate. Honeycomb from three different shanks were cut to get three uniform specimens from each shank. Two of the shanks came from countermine boots and the other shank came from of a countermine overboot.

---

[1] *Compressive direction* was the direction downward on the sole. *Ribbon direction* (longitudinal direction) was the direction in which the sheets of aluminum ran. [heel-to-toe] *Transverse direction* was the direction in which the aluminum sheets were bonded. [side-to-side on the foot]

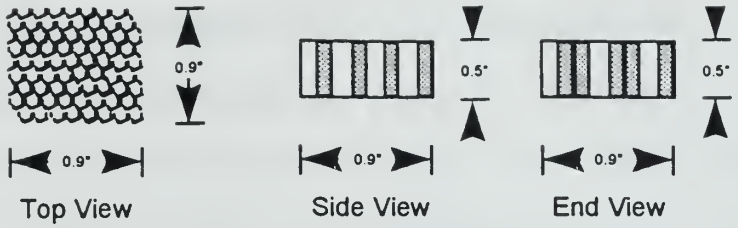

Figure 5.2 Diagram of honeycomb specimen.

2. Test Procedure

The test procedure was to gather compressive material properties on the honeycomb. The honeycomb was compressed on all three axes (that is, in all three directions). Each sample was compressed beyond the point at which the honeycomb failed and was continued until the honeycomb became nearly solid. Stopping the test at this point seemed prudent since all useful data was obtained early in the test and continuing the test risked damage to the Instron machine.

C. STAINLESS STEEL PREPARATION AND TEST PROCEDURE

1. Specimen Preparation

The stainless steel used on the top of the shank was considerably thinner than that used as the bottom of the shank, 0.02 in versus 0.06 in. ASTM E8-96, Standard Test Methods for Tension Testing of Metallic Materials [Ref. 8], specifies the standard "dog bone" shape to be used depending upon the thickness of the material. It was recognized that

precise specimen preparation would be difficult with very thin samples. Acknowledging that the top piece of steel was thin, it was determined that if both steels were proven to be the same only the thicker steel would have to be cut and tested to find the material properties of both. With the Scanning Electron Microscope (SEM) and the Energy-Dispersive X-ray (EDX) machine, this was proven to be the case. (See Appendix A for this procedure and discussion of results.)

With only the thicker steel to test, the next task was to determine the dimensions of the sample. As was the case with the rubber, the ASTM required more material than was available. Therefore, the dimension were again scaled proportionally and cut using an Electrical Discharge Machine (EDM)[2] to ensure accuracy. The dimensions used can be seen in Figure 5.3. Three of these specimens were cut. One was from one blast boot and the other two were from the same shank in a different blast boot.

2. Test Procedure

This test was to gather tensile material properties of the specimens. The test procedure outlined in E8-96 is very specific on the procedure depending upon desired data, gauge

---

[2] *Background on the EDM:* The EDM is often used to cut high strength, electrically conductive materials to precision. The fundamental process of the machine is to use flowing, electrically charged water to induce an electrical charge in the material. An electrically charged, moving wire then cuts through the material along the desired path at a very slow rate. While passing through the material, this thin wire is essentially melting the material and cutting out the desired/ programmed shape. The code used to program the EDM is a simple DOS-based code.

length of the specimen, size of extensometer, etc. One concern was possible slippage in the grips since the specimen, while thicker than the top steel was still a relatively thin sample. Therefore, each specimen was cleaned with acetone to ensure the removal of all epoxy and rubber residue left from the removal from the boot. The specimens were then placed in common wedge-shaped grips in the Instron machine. This wedge shape is designed to encourage a tight grip as force is applied and extension, as well as thinning, of the specimen occurs. Given the expected high strength of the steel, an extensometer was attached to the specimen to ensure accurate readings of initial displacement. (While the Instron machine is accurate at obtaining data, using an extensometer to gather the data in tensile tests is more accurate.) In accordance with ASTM E8-96, an extensometer with a gauge length smaller than the gauge length of the specimen was selected, 0.5 vs 0.8 in, respectively.

The cross-head speed recommended by ASTM E8-96 correlates to a strain rate between 0.05 in/in/min and 0.5 in/in/min. Given the dimensions of these specimens, a strain rate of just under 0.5 in/in/min equated to a cross-head speed of 0.05 in/min. Due to limitations on the extensometer used, data collection switched from the

extensometer to the Instron machine at 4% strain. This proved to work out quite

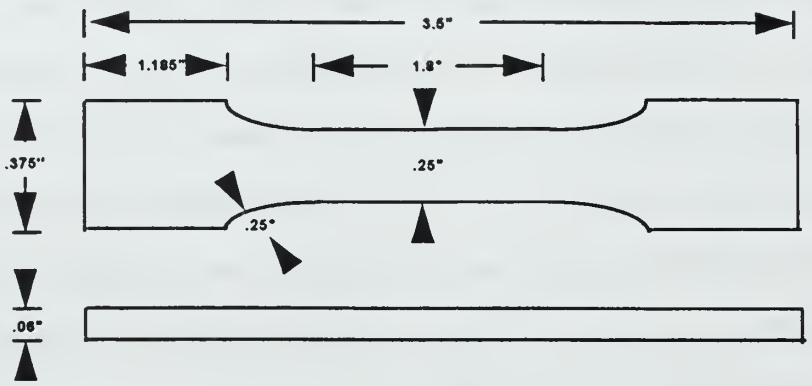

Figure 5.3 Diagram of steel specimen

well and the extensometer was able to record data beyond the point at which the yield force was reached. The testing was continued until failure of the specimens occurred.

D. KEVLAR PREPARATION AND TEST PROCEDURE

1. Specimen Preparation

Testing for material properties of the kevlar was expected to be the most difficult. With no information on the type, weave, or size of the fibers, no information on the resin used, and no accurate way of counting the number of layers of the weave, there was essentially no way of calculating properties of the kevlar using common equations used for orthotropic composites. Therefore, macrotesting was the only way to get the desired properties. In ASTM

D3039/D3039-95a, Standard Test Method for Tensile Properties of Polymer Matrix Composites Materials [Ref. 9], recommended dimensions of test specimens. Again, however, the ASTM dimensions for test specimens had to be scaled proportionally to accommodate the available material using desired gauge lengths as a basis. Given the limited dimensions of the material, gauge lengths of 0.75 in and 1.5 in were established for the transverse and longitudinal test specimens, respectively. Test specimens to be used for testing of transverse properties were 0.25 in wide. Test specimens for testing longitudinal properties were proportional and 0.5 in wide. The reason these width dimensions varied was to ensure an adequate number of test specimens (three) in each direction given the shape of the sole and the required overall length of the specimens based on the scaled ASTM dimensions. Grip lengths were also a concern since it was a concern that the specimens could slip in the grips. The dimension listed in Figure 5.4 allowed for grip lengths of 1.475 in and 2.0 in for transverse and longitudinal test specimens, respectively. The specimens were cut along the seams of the kevlar fabric since the seems of the fabric are longitudinal and transverse when the liner is placed in the boot.

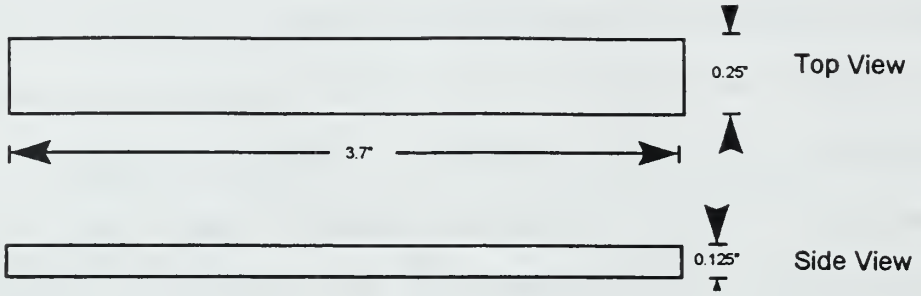

a.) Transverse specimen.

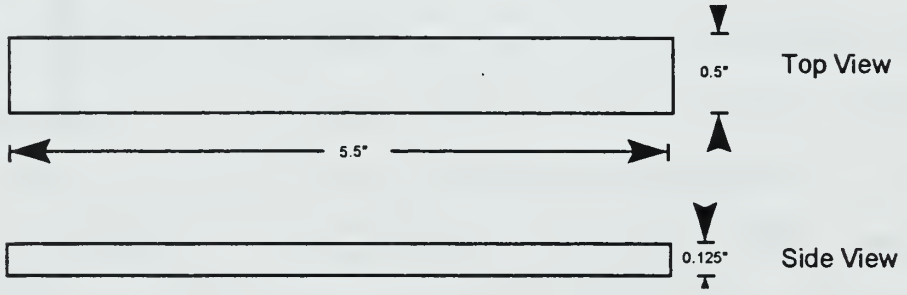

b.) Longitudinal specimen.

Figure 5.4 Diagrams of kevlar specimen.

2. Gripping and the Use of Tabs

Many material configurations such as multi-directional laminates and fabric-based composites cannot be successfully tested without tabs. The use of tabs prevents stress concentrations from developing at the machine grips. This concentration of stress may cause the specimen to fail at the grips rather than in the test region. The ASTM further recommends their use when testing unidirectional materials to failure when slippage in the grips occurs. A table provided in ASTM 3039/3039M lists tab dimensions based on

the dimensions of the test specimen. Tabs were manufactured out of aluminum. Dimensions used can be seen in Figure 5.5.

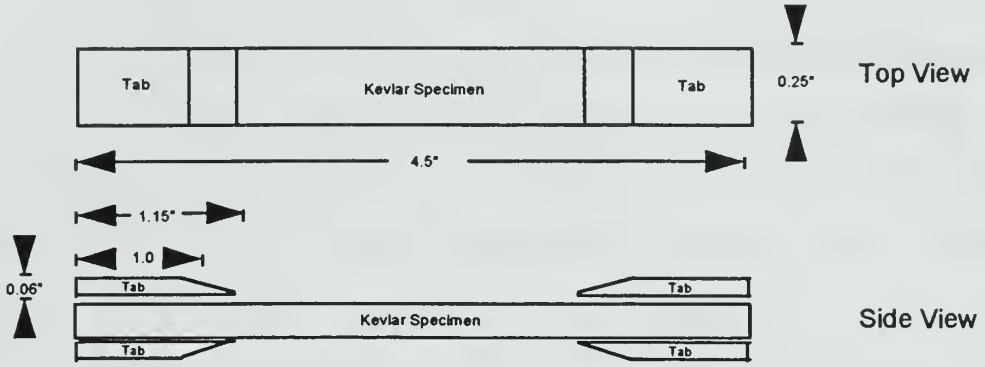

Figure 5.5 Diagram of tab dimensions.

The tabs were bonded to the kevlar specimen using a two-part industrial strength epoxy. After mixing M-Bond type 10 curing agent into M-Bond adhesive resin (Type AE), the epoxy was place between the tabs and the specimen. The specimen was then clamped in a vice and allowed to set overnight.

3. Test Procedure

The use of ASTM 3039 test method works well for orthotropic specimens. This is due to the uniform state of stress that is produced as tensile loading is induced [Ref. 10]. The testing on the kevlar was to obtain tensile material properties in both the transverse and longitudinal directions. The test procedure was conducted like that used for the steel specimens.

The cross-head speed to be used is also specified in ASTM 3039/3039M and, like the tensile testing of the steel, is given in terms of strain rate. In this case, the recommended speed should be such that failure is produced in one to ten minutes. The ASTM further recommends that if failure points are unknown, a standard head displacement rate of 0.05 in/min is recommended. A speed of 0.1 in/min was found to produce failure within the limits specified above (normally between five and seven minutes).

VI. TEST RESULTS

A. TEST RESULTS OF RUBBER

The primary goal of the rubber compression testing was to obtain accurate data on the elasticity of the rubber used in the boots and compare this data for different boots. The stress vs strain plots for the rubber samples are enclosed as Appendix B.

As stated previously, the raw data from the Instron machine's computer was downloaded as an ASCII file of data points in the form of force (lbs) and displacement (in). In MATLAB, this data was converted to stress and strain. This data was then plotted to simplify comparison of the specimens. (See Appendix C.) It is clear that the rubber from the specimens of each boot behaved almost identically, regardless from which boot the specimen originated.

The initial linear region was linearized in MATLAB in order to most accurately calculate a Young's modulus of elasticity. The Young's moduli are listed in Table 6.1. It is noteworthy that all of the Young's moduli, with the exception of the first sample of the first boot, are within 5% of the average. If the first boot's first sample was discarded, the average Young's modulus would be 1603.9 psi. The remaining five samples are all within 3.8% of this value.

Table 6.1 Test results of rubber testing.

Boot	Sample	Young's Modulus (psi)
1	1	1416.1
1	2	1544.5
1	3	1647.3
2	1	1623.0
2	2	1561.1
2	3	1643.7
	Average	**1572.6**

In addition to having such close Young's moduli, all of the samples' elastic regions lasted until strain values were approximately 0.3 in/in.

B. TEST RESULTS OF ALUMINUM HONEYCOMB

The most critical values to be obtained from the compressive tests of the honeycomb specimens was the failure strength of the honeycomb in the compressive/downward direction. That is, at what pressure the honeycomb will begin to collapse in the vertical direction. Plots of the stress vs strain curves are given in Appendix C. The results for failure in all three directions are given in Table 6.2. It is clear that the vertical strength of the honeycomb is far greater than the strength in either longitudinal or transverse directions.

Table 6.2 Test results of honeycomb testing (Failure Strengths).

	Vertical (psi)	Transverse (psi)	Longitudinal (psi)
Overboot Shank	4649	148	244
Boot #1 Shank	4643	169	201
Boot #2 Shank	5196	181	219
Average	**4829**	**166**	**221**

As was done with the rubber specimens, the initial region was linearized utilizing MATLAB. These equations were then used to calculate Young's moduli for each sample in each direction. The results are given in Table 6.3. It is interesting to note that the values obtained from the overboot shank in the downward and longtudinal directions are considerably different than the other samples which are relatively close. This could be the result of weaker bonding between the sheets of aluminum that make up the honeycomb. Since the failure strength, not Young's modulus, was considered the most critical property and given the limited amount of sampling material, no effort was made to test additional samples to find out if other honeycomb samples would behave the same as the overboot sample.

Table 6.3 Test results of honeycomb testing (Young's Moduli).

	Downward Young's Modulus (psi)	Transverse Young's Modulus (psi)	Longitudinal Young's Modulus (psi)
Overboot	95,500	13,290	3908
Boot #1	164,900	6616	4960
Boot #2	127,450	6418	4950
Average	**129,283**	**8775**	**4606**

C. TEST RESULTS OF STAINLESS STEEL

The steel testing was unlike the two previous tests because not only was it a tensile test but some information about the steel was known prior to the test as a result of the EDX discussed above. Additionally, one test specimen came from one boot (Boot #1) while the other two samples came from a second boot (Boot #2). The values found for the three tensile tests are listed in Table 6.4.

Given the purpose of the blast boots, the critical properties can be considered the yield strength and the ultimate strength. Due to the EDX finding that the steel for both the shank upper and base was Type 302 stainless steel, the values in Table 6.4 can be compared to any number of references. Depending on the amount of cold-working imposed on the steel during manufacturing, the values for .2% yield strength are within accepted values ranging from 30,000 psi [Ref. 11] to 75,000 psi [Ref. 12] if it has been cold-worked. This is also true for the values of ultimate

Table 6.4. Test results of steel testing.

	0.2% Yield Strength (psi)	Ultimate Strength (psi)	Young's Modulus (ksi)
Boot #1	36,710	95,818	26,300
Boot #2, Sample #1	39,370	99,070	29,700
Boot #2, Sample #2	40,040	99,270	31,200
Average	**38,707**	**98,052**	**29,066**

strength. Expected values ranged from 90,000 psi [Ref. 11] to 110,000 psi [Ref. 13]. Clearly, the test values obtained for these properties are very accurate.

References indicated that modulus of elasticity should be approximately 28 x 10^6 psi [Ref. 14]. A plot of the elastic region of the stress vs strain curves for the three specimens is given in Appendix E. It can be seen that Young's modulus for Sample 1 (Boot #1) is lower than that of the other two specimens. It is important to mention that of all the data obtained, there will be more error associated with obtaining an accurate Young's modulus than any other. This is primarily due to possible slippage in the extensometer and inherent error in using a screw-type machine to accurate data early in a test.

D. TEST RESULTS OF KEVLAR

The tensile testing results for the kevlar specimens are given in Table 6.5. Stress vs strain curves for the

specimens are given in Appendix E. As noted in Table 6.5, the first transverse specimen's tabs failed at some point during the testing. In fact, three of the four tabs failed. More accurately, the epoxy between the tabs and the specimen disbonded. This may have caused some degree of at slippage at the point when disbonding occurred. Without knowing the point at which this happened, the resulting data was regarded as unreliable. Data is included in Table 6.5 only for comparison.

As a result of the failure of the tabbing process and given the limited number of samples, it was decided that tabs would not be used for the following specimen. This was based on earlier, preliminary testing to determine the appropriate crosshead speed that resulted in the failure of that specimen within the test region without the use of tabs. The second specimen failed in the test region as desired so it was decided to not use on the final specimen. As seen in Table 6.5, the second and third transverse specimen test results are extremely close.

As a result of lessons learned on the use of tabs in testing the transverse specimens, it was decided to not use tabs on any of the longitudinal test specimens. Unfortunately, the Instron machine's control panel experienced a software malfunction during the second test. The result was that the machine stopped recording displacement as the specimen was loaded. For this reason,

Table 6.5. Test results of transverse kevlar tests.

	Maximum Stress (psi)	Young's Modulus (psi)
Specimen #1	42,378*	239,560*
Specimen #2	44,884	106,320
Specimen #3	45,717	108,840
Average	**45,300****	**107,580****

* Tabs failed.
** Includes data from specimens 2 and 3 only.

no Young's modulus was obtainable. However, the load applied to the specimen was recorded so failure stress was obtained and should be considered as accurate. Longitudinal test results are given in Table 6.6.

Table 6.6. Test results of longitudinal kevlar tests.

	Maximum Stress(psi)	Young's Modulus (psi)
Specimen #1	45,412	374,850
Specimen #2	42,633	*
Specimen #3	39,788	255,770
Average	**42,611**	**315,310****

* Instron machine malfunctioned.
** Includes data from specimens 1 and 3 only.

The failure stress for both transverse and longitudinal directions should be considered to be the same. This was expected since the layers of the kevlar are applied in a

0/90 manner. That is, each layer is applied perpendicular to the preceding layer.

VII. FINITE ELEMENT MODEL

A Finite Element Model (FEM) was developed to analyze the response of the countermine boot to the blast generated by an M-14 mine and measure the boot's ability to dissipate the overpressure created by such a blast. The model was constructed utilizing the windows-driven PATRAN preprocessor. This program allows for easy manipulations of complex geometries. Once the mesh was generated in PATRAN, it was exported to DYNA-3D, version 9.36. DYNA-3D was used as a processor and simulated static and dynamic conditions. It was capable of modelling the behavior of the materials subjected to various loads.

Figure 7.1 shows the longitudinal and transverse cross-sections of the countermine boot. For the purposes of modelling this boot, the boot was simplified to focus on the a 3 in x 3 in cross-section centered on the heel and ankle. As seen in Figure 7.2a, the FEM mesh included the individual components of the countermine boot and also included a mesh to simulate the tibia (the largest bone extending from the ankle to the knee). Figures 7.2b through 7.2e show the pieces of the model that represented the various components of the boots. The boot shape was further modified to discount the rubber stabilizers along the outside edges of the sole. This was to make it easier to apply a blast force to the base of the boot and thereby exerting a force axially force to the bone. The countermine boot material

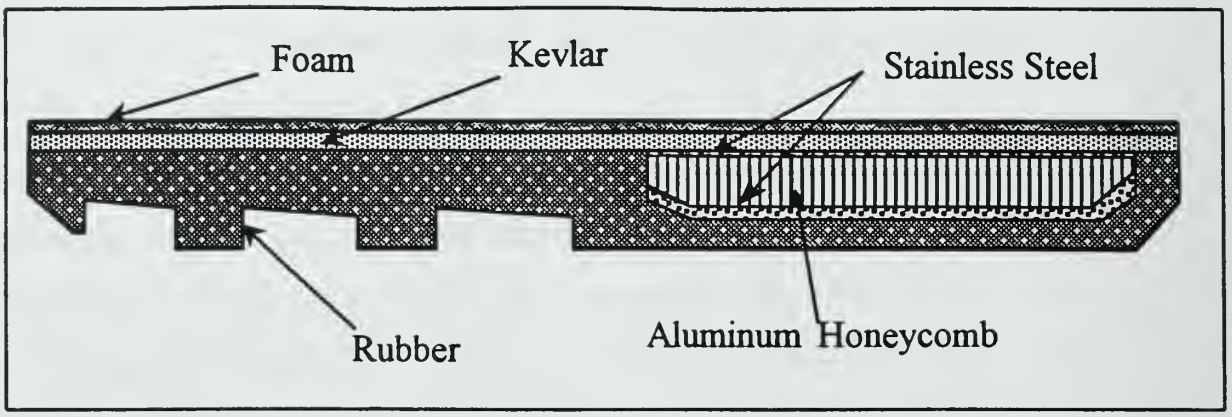

a. Longitudinal cross-section

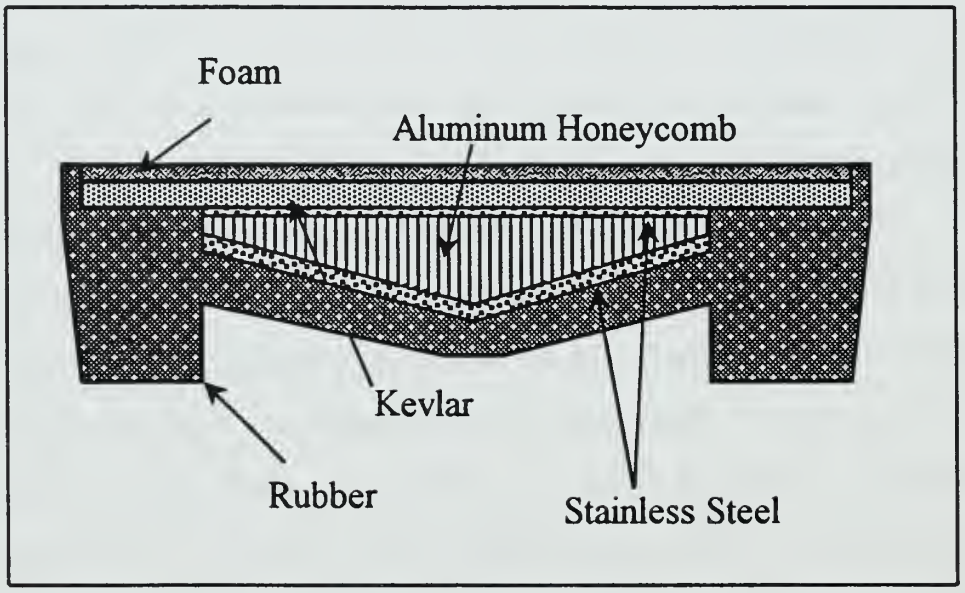

b. Transverse cross-section.

Figure 7.1 Longitudinal and transverse cross-sections of the countermine boot.

properties used in this simulation were those obtained in the static testing conducted for this project described

previously (Chapter VI). Material properties for the bone were obtained from open literature.

Time of detonation of the mine was taken as the initial or zero time. At this time the model was subjected to a pressure wave consistent with those generated by an M-14 AP mine. In this preliminary model, the pressure wave is represented by a normally incident wave with a duration of 0.0715 ms and a peak pressure of 1941 psi. A load curve has been defined to describe the pressure as a function of time using Equations 7.1 and 7.2 [Ref. 3].

$$\frac{p_o}{p} = \frac{808 * \left[1 + \left(\frac{Z}{4.5}\right)^2\right]}{\sqrt{1 + \left(\frac{Z}{0.048}\right)^2} * \sqrt{1 + \left(\frac{Z}{0.32}\right)^2} * \sqrt{1 + \left(\frac{Z}{1.35}\right)^2}} \qquad (7.1)$$

where

$$p = p_o * \left(1 - \frac{t}{t_d}\right) * e^{-a * \left(\frac{t}{t_d}\right)} \qquad (7.2)$$

Figure 7.2a Entire finite element model.

Figure 7.2b Finite element model of kevlar liner.

Figure 7.2c Finite element model of stainless steel.

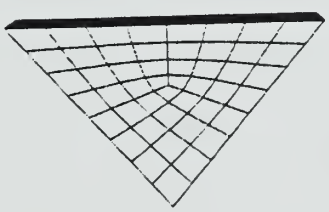

Figure 7.2d Finite element model of aluminum honeycomb.

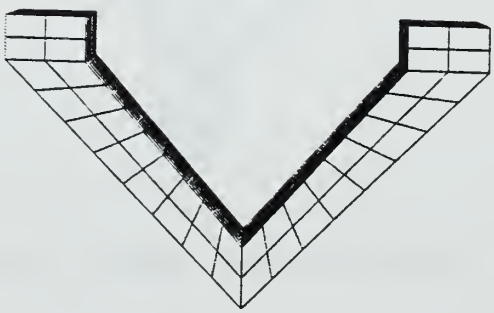

Figure 7.2e Finite element model of rubber sole.

VIII. UTILIZING THE FINITE ELEMENT MODEL

A. VALIDATION OF THE FINITE ELEMENT MODEL

After the finite element model (FEM) was developed, the next step in this analysis was to validate its accuracy using real-world test data and comparing it to data generated by the model. We were able to obtain a test report detailing the results of a test conducted at the U.S. Army Aberdeen Test Center (Test Record No: LFV-27-97) in order to validate the FEM. This test included sufficient data to verify our model. Specifically, the testing involved exploding one ounce of C-4 under a countermine boot. Peak force and peak impulse data were obtained as well as a force versus time graph. There were, however, some approximations still necessary to complete the comparison between our FEM and Aberdeen's results. Such approximations included estimating the material properties of the polyethylene bar connecting the boot to the force meter, the exact distance between the force meter and the boot, etc.

Applying a load equivalent to one ounce of C-4 to our model resulted in very similar output in a force vs. time graph as that obtained at Aberdeen. Figure 8.1 compares the results of our FEM to the results of Aberdeen's test. The element selected for the FEM curve was an element 15 inches

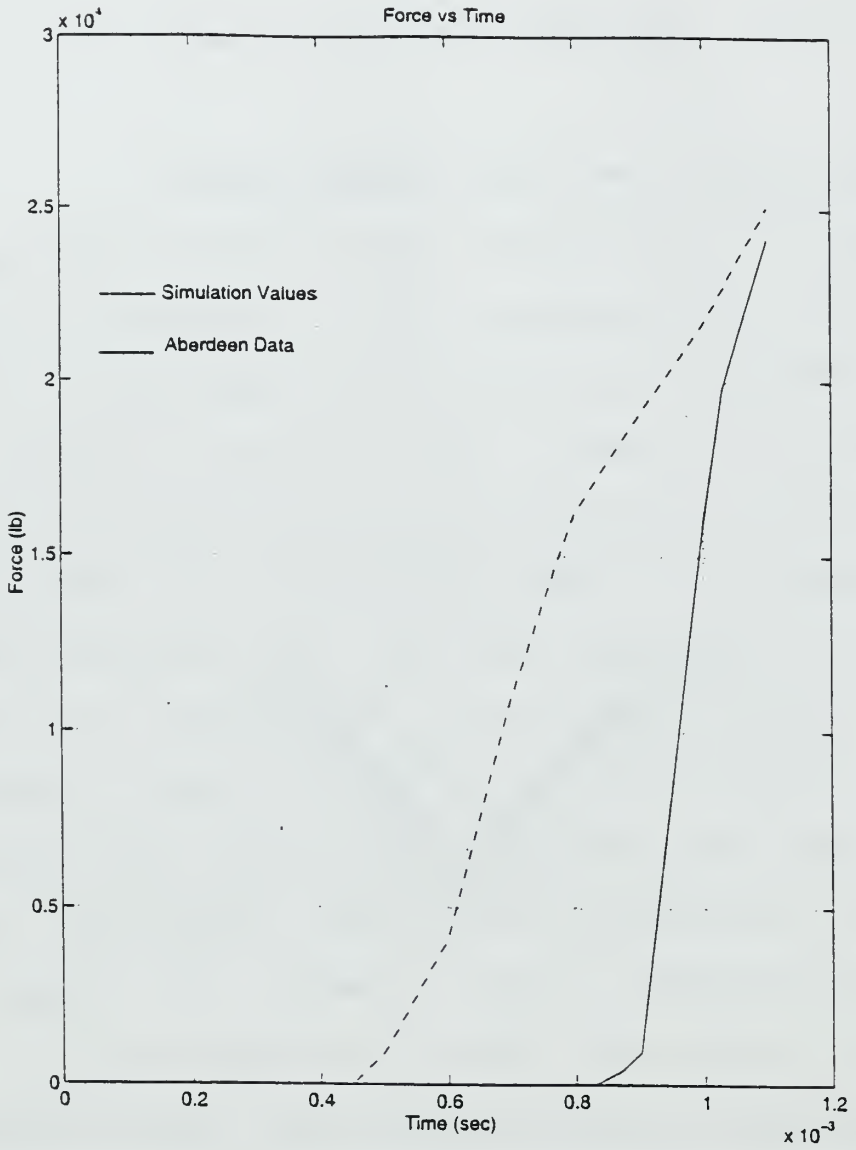

Figure 8.1 Comparison of Aberdeen test data and FEM data.

above the sole of the boot. This was the distance approximated between the force transducer and the sole of the boot based on our analysis of a photogragh of the actual test setup. As can be noted from the Figure 8.1, the initiation of stress at that location for the model was approximately 4 milliseconds earlier than the Aberdeen test.

Also, the maximum force experienced is slightly higher in the FEM (25,083 lbs vs 23,910 lbs). Our FEM peak force is 5% greater than the Aberdeen test. This variation was not considered significant and, therefore, the model was accepted as being able to represent the real-world test.

There are many realities of blast loading/testing and inherent variations associated with blasts of equal origins that contribute to such discrepancies. Blast testing values will never produce exactly the same values from one test to another. The complex dynamics involving the extreme overpressures in the immediate environment of a blast and the behavior of materials when subjected to real world blasts are never exactly repeatable. The model disregards imperfections in the materials and environment that may exist in real world test. Additionally, the model assumes perfect interfaces between the layers of materials in the blast boot. This assumption will increase the speed of wave propagation as seen in our model.

If Aberdeen ran additional tests on a similar boot with a similar blast charge, the results would undoubtedly vary from its initial results. For this and the reasons mentioned above, the model was accepted as producing quantitatively accurate values for peak forces.

B. BLAST EFFECTS ON COUNTERMINE BOOTS

Prior to initiation of the model, it was expected that we should be able to observe the deformation of the boot as the blast wave passed through it. Accompanying this blast wave should be an associated increase in stress. For the purpose of this analysis only a few timesteps will be discussed to demonstrate that the model deformed as expected as the higher stress loads progressed through the boot. In this case, we will focus our analysis of stress on the von Mises effective stress.

Deformation of the boot can be seen in Figures 8.2 through 8.5. As seen in Figure 8.2, prior to application of the blast wave, the boot was in no way deformed. Figure 8.3 shows that at 0.5 msec the pressure on the sole of the boot is sufficient to cause initial deformation not only of the rubber but of all other components. It can be seen that the aluminum honeycomb in the center of the shank has begun to collapse. Figure 8.4 shows deformation at 0.7 msec and indicates a continued progression as the rubber has compressed significantly and the honeycomb continues to be crushed. Figure 8.5 indicates severe deformation at 1 msec. Particularly noteworthy are the way in which the honeycomb has collapse and the deflection of the kevlar lining on top of the sole. As this deflection has increased, stress in the element just above this kevlar (representing the stress

felt on the sole of the foot) have increased. This progression of increased stress on these elements will be addressed later. Deformation continues in this manner until approximately 1.6 msec.

The von Mises stresses associated with the time discussed above can be seen in Figures 8.6 through 8.8. This increase in stress behaves as expected. Initially, the highest stresses are observed to be at the base of the shank. However, as time and deformations continue the region with the highest level of stress is most concentrated at the interface between the kevlar lining and the bone material.

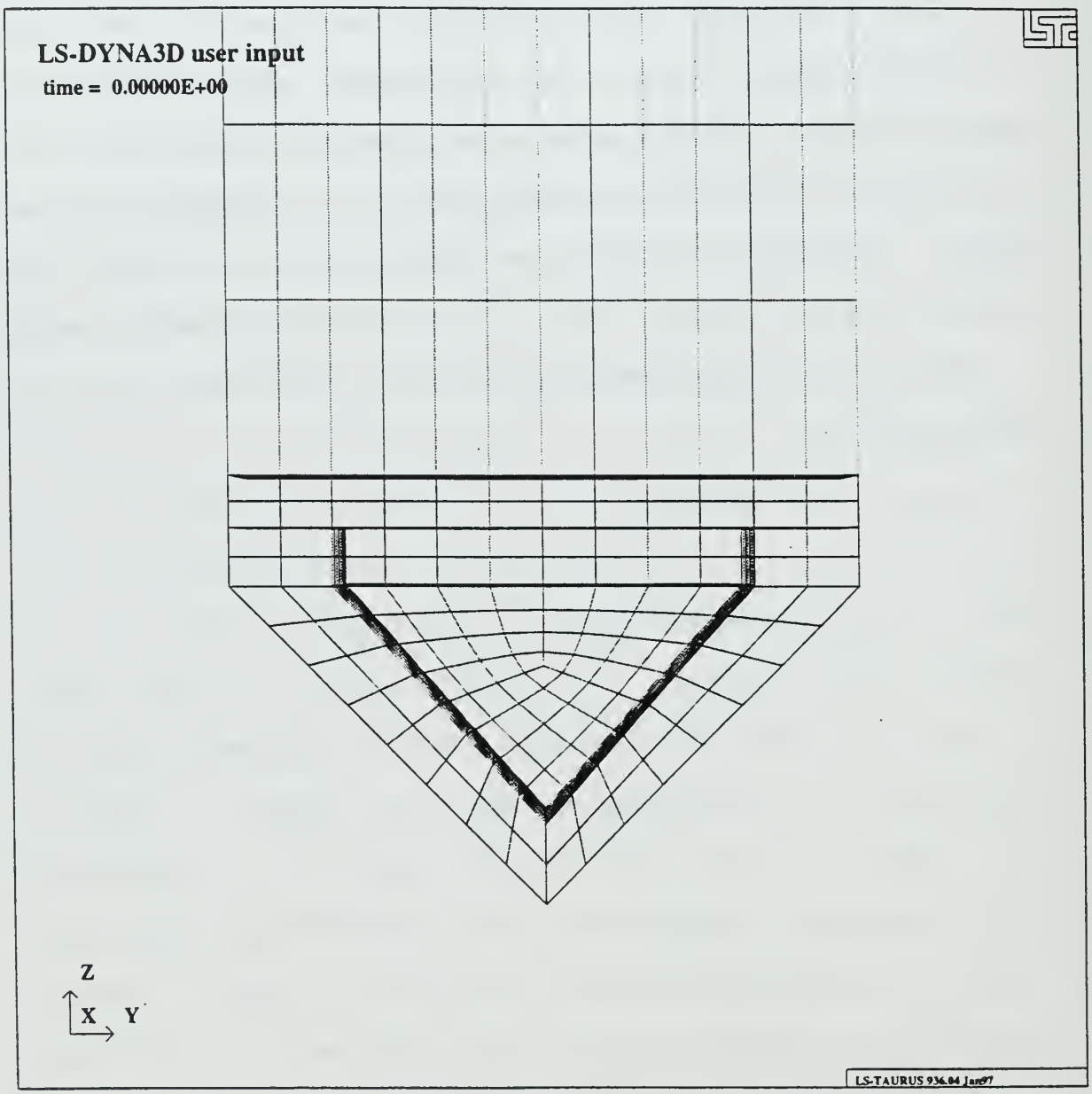

Figure 8.2 The finite element model prior to application of the load.

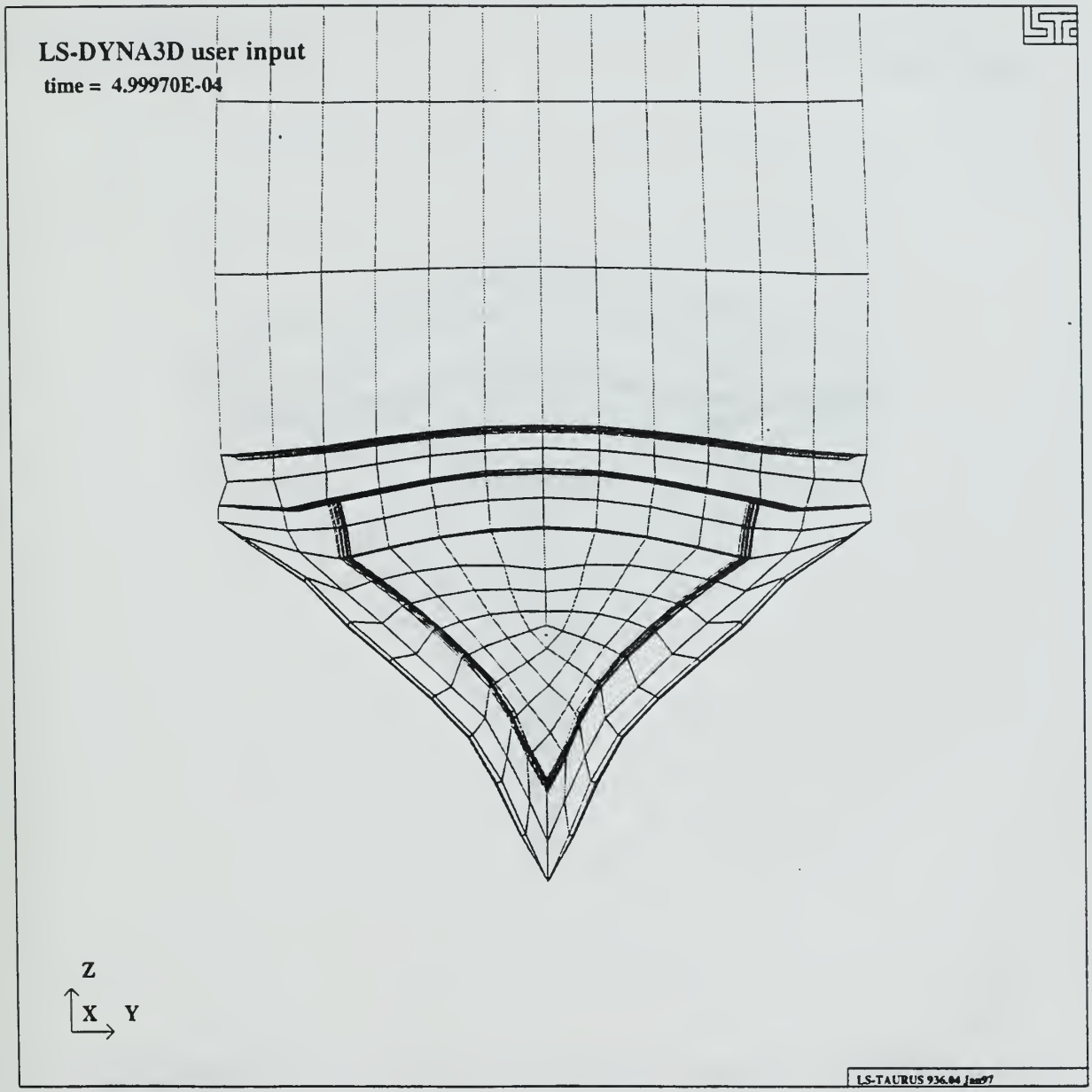

Figure 8.3 Deformation of the boot at approximately 0.5 milliseconds.

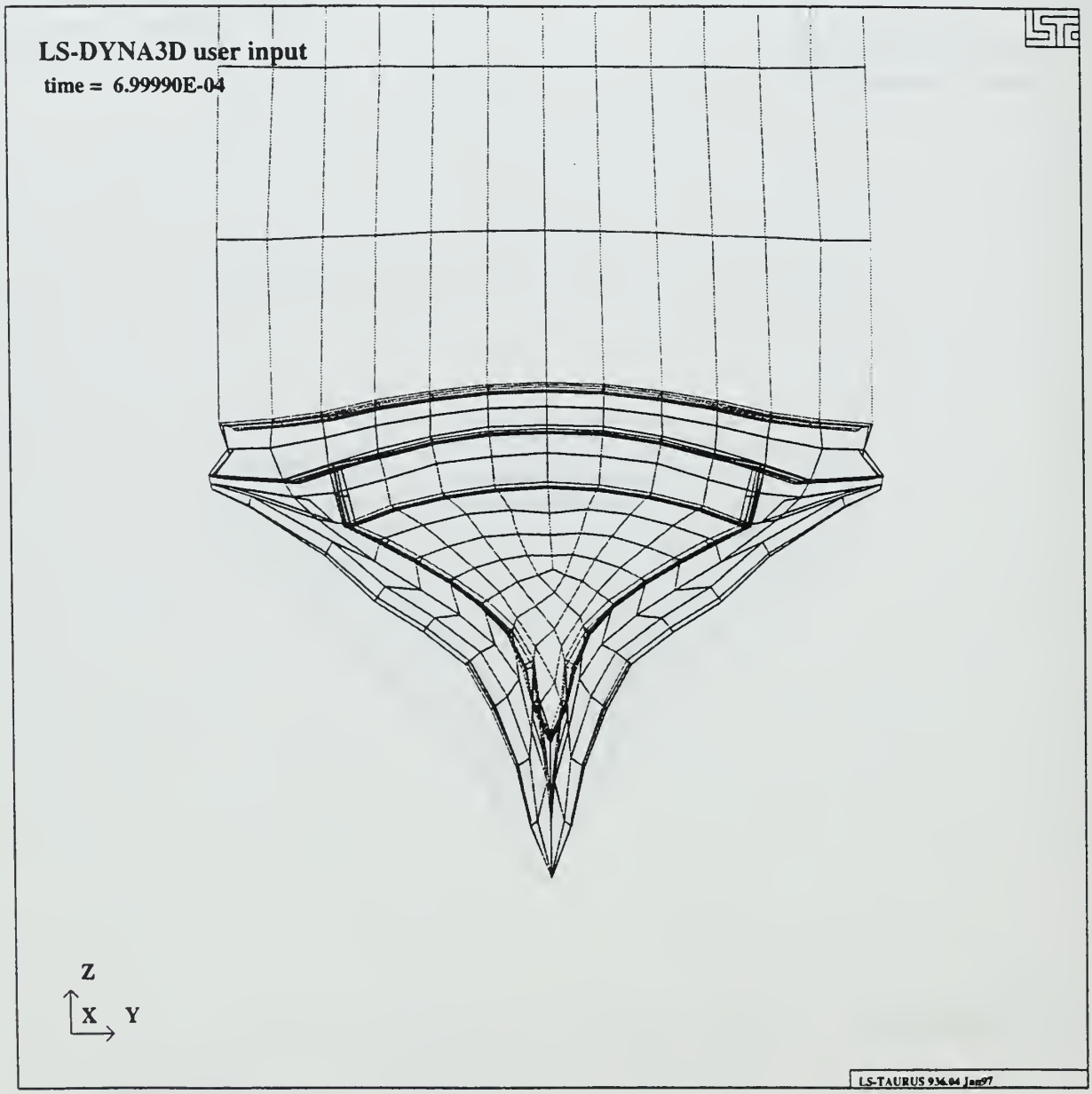

Figure 8.4 Deformation of the boot at approximately 0.7 milliseconds.

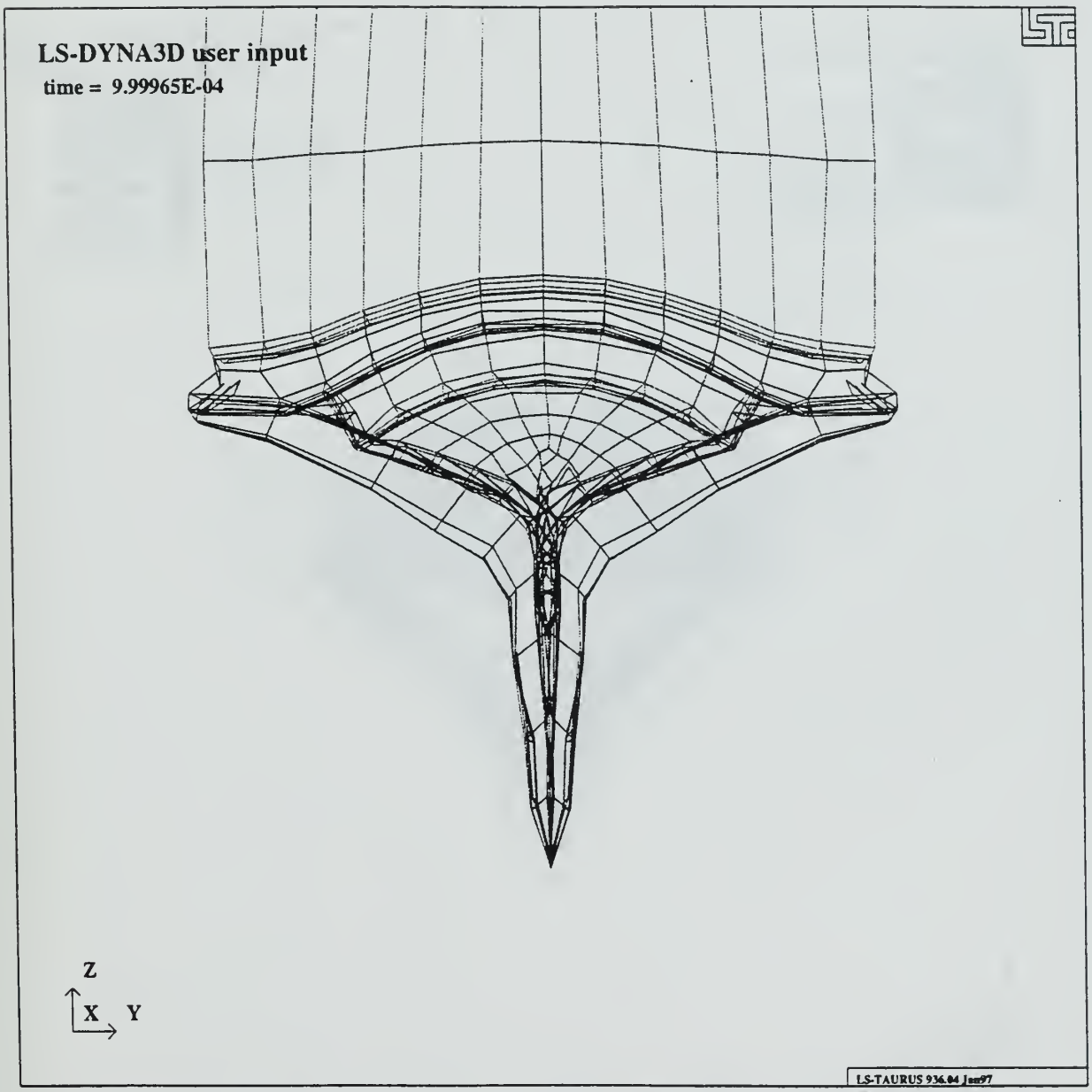

Figure 8.5 Deformation of the boot at approximately 1.0 milliseconds.

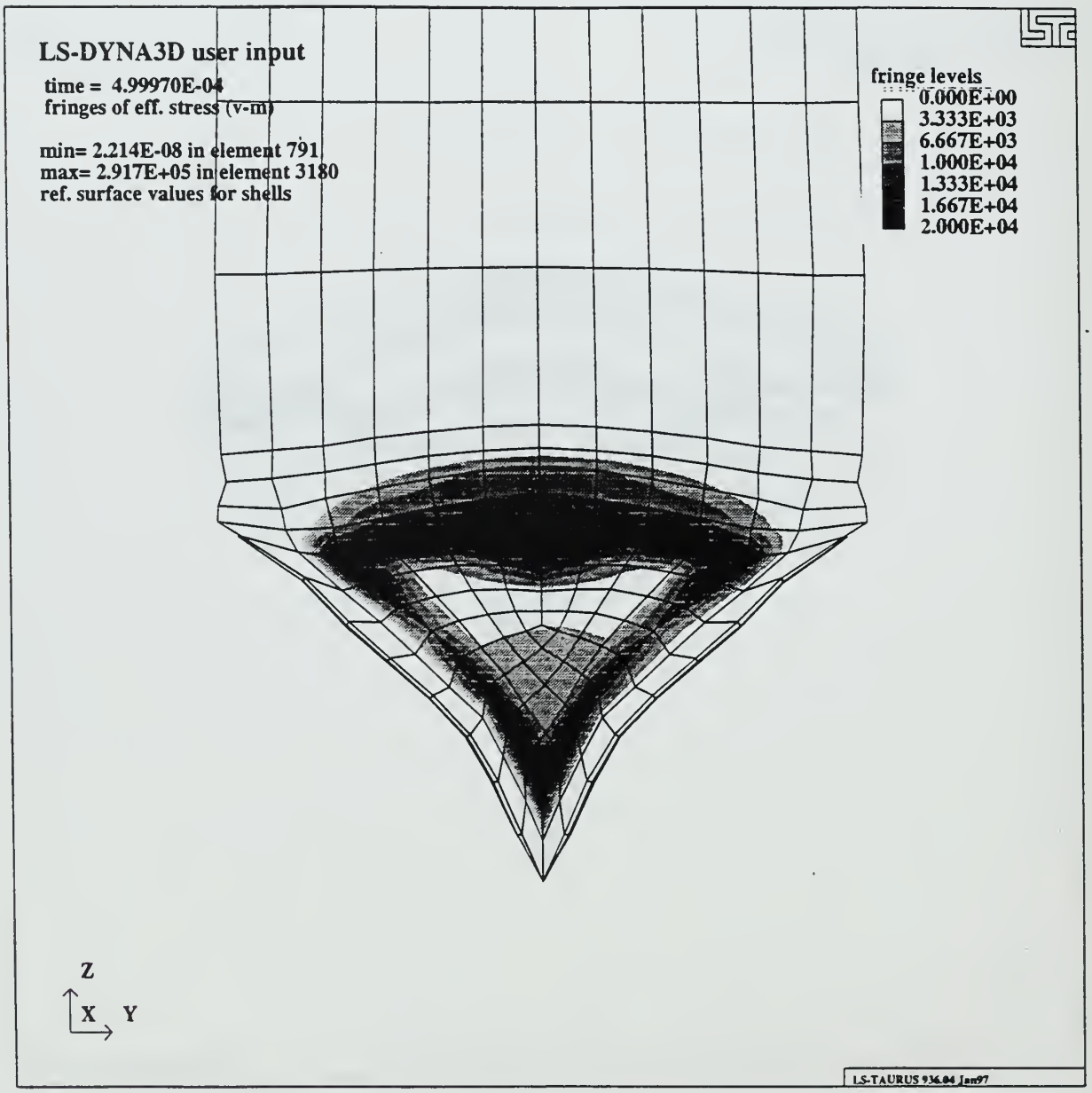

Figure 8.6 Von Mises stress across the boot at approximately 0.5 milliseconds.

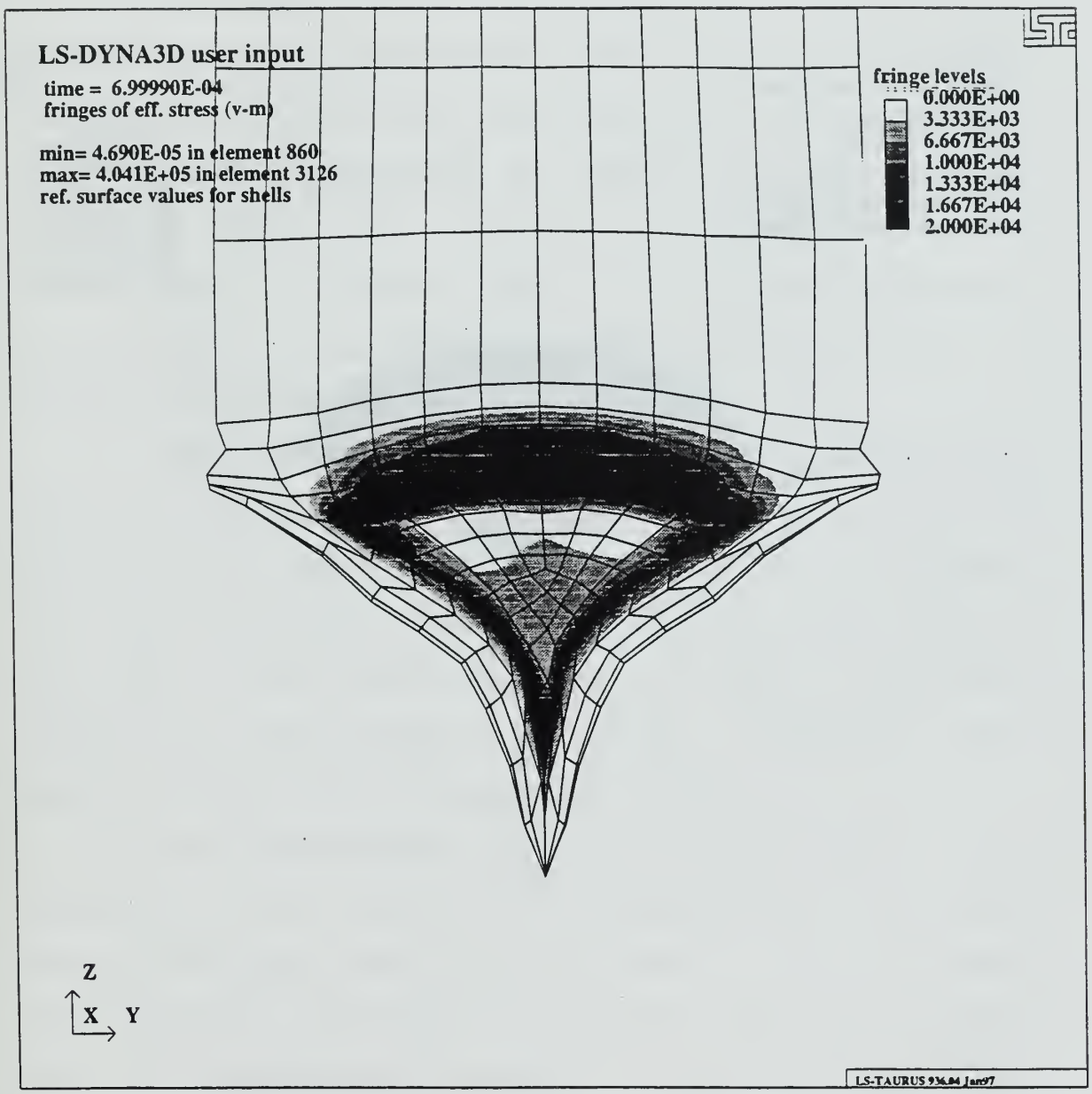

Figure 8.7 Von Mises stress across the boot at approximately 0.7 milliseconds.

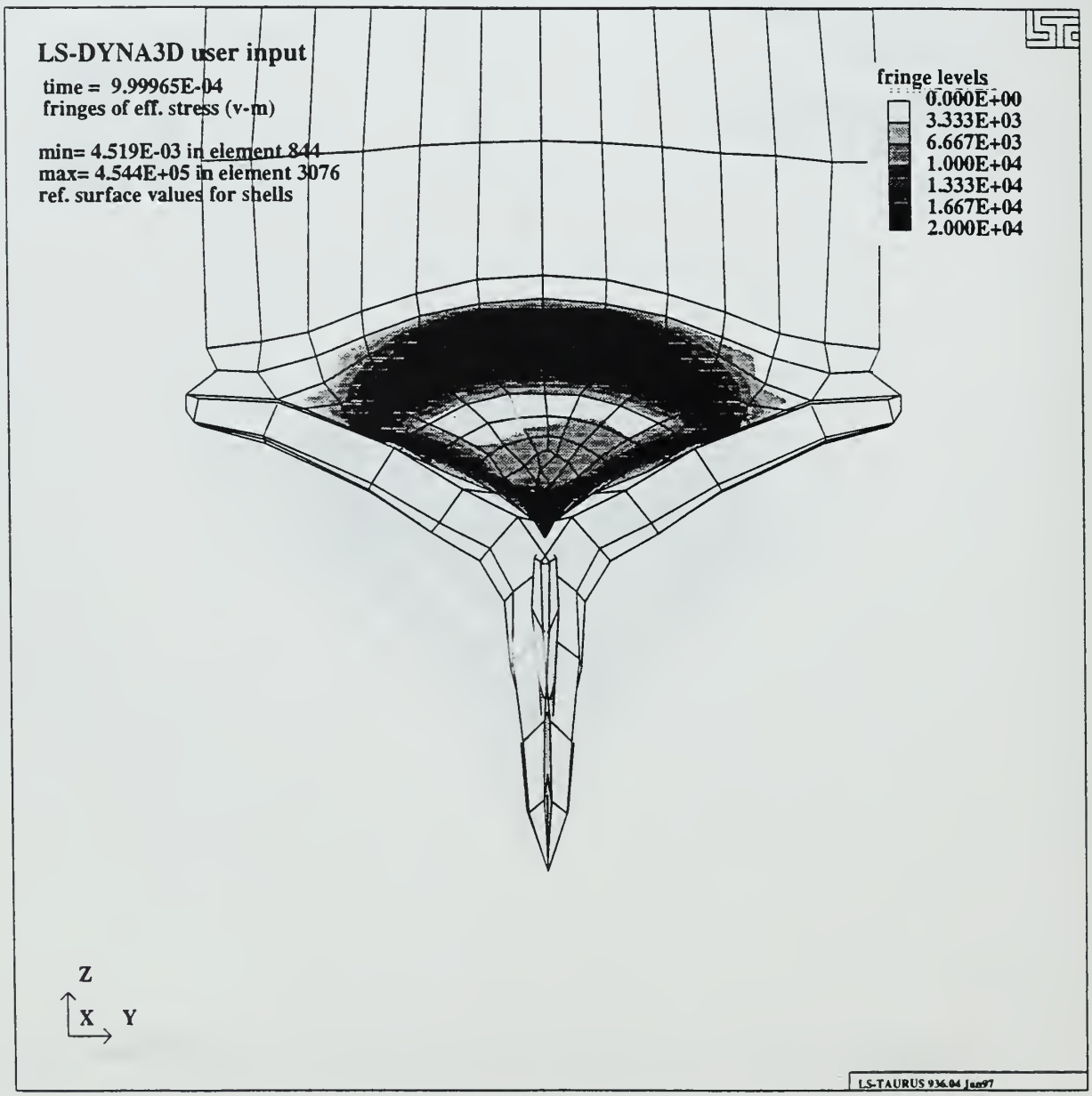

Figure 8.8 Von Mises stress across the boot at approximately 1.0 milliseconds.

C. BLAST EFFECTS ON THE LOWER EXTREMITIES

This model attempts to represent the mechanical properties of the lower extremities by a skeletal frame of bone only. Material properties for the tibia were used for the entire section of the leg. Follow on models should include the fibula and the the soft tissue to give a more accurate view of the energy absorbing properties of the leg. The mechanical properties of bones and other organic materials vary and dependent on many different circumstances. The values used for this model are nominal values adopted from available literature to represent an average of properties [Ref. 15].

It is critical to recognize that biomechanical properties can vary greatly depending on not only gender and age such that a young male is more likely to have stronger bones than an older female. Bone structure also plays a major part in the overall strength of a bone. Some people simply have larger bones than others. Therefore, their bones are most likely stronger than average.

For the determination of a critical axial force required to break the tibia it was assumed that the person wearing the boots was a mid-size male. It is extremely important that the reader understand and appreciate the range of biomechanical properties of bones in humans. For instance, a small female's tibia may fail under an axial load of 5200 pounds of force. Whereas a large male may require a value as high as 9900 pounds. For the purposes of

this study, a mid-size male's tibia will fail under an axial load 8070 pounds [Ref. 15]. Further properties of the bone used for this model are listed in Table 8.1.

Table 8.1: Properties of Human Bone used in FEM Model. From Ref. [16]

Density	0.018 lb/in^3
Young's Modulus	15,000 psi
Poisson's Ratio	.3
Critical Failure Force	8070 pounds

Given these bone properties, the current design of the countermine boot was analyzed. The application of a load equivalent to an M-14 AP mine was applied to the bottom of the boot. At approximately 1.6 msec, the resulting blast force on the base of the tibia reached a maximum value. This value of this force was 6,885 pounds.

Therefore, it was determined that that the current boot design offered a considerable reduction in force as the blast wave passed through the boot and shank. However, while this value of 6,885 lbs was below the critical value established for a mid-size male (8,070 lbs), it was higher than the critical value established for a small female (5,200 lbs).

It remains critical to recognize that the elastic and ultimate properties listed above may possess inherent inaccuracies that are associated with all bone biomechanical

properties. Large variations in moduli and strengths have been reported throughout reference literature due to the differences in testing methods and significant differences in the bone architecture. These differences are linked to the anatomic location, age and testing direction of the test specimen. Variations as high as two orders of magnitude have been found within specimens from one individual. This exemplifies the difficulties associated with assessing bone properties. [Ref. 16]

Therefore, although the value of the 6885 lb force exhibited by the current model is lower than the 8070 lb critical value established, damage and/or failure of the tibia is still possible. These values are of the same order of magnitude and it should not be assumed that the current boot offers an acceptable level of protection for the lower extremities. Thus, if is possible to reduce the current transmitted force, this should be done.

D. VARIATION OF MATERIAL PROPERTIES AND DIMENSIONS

Following the determination of the maximum force on the tibia allowed by the current design of the countermine boot, the next step in this analysis was to determine the results of varying the material properties of the current design. ("Current design" here implies that the overall shape of the boot and its components will not be altered.) In addition

to changing the properties of the shank components, the thicknesses of the shank components were altered to determine the impact on overall force dissipation. First, the stainless steel casing of the shank was altered. The "base" of the casing (the bottom V-shaped portion of Figure 7.2c) and the "top" of the casing (the flat, horizontal shell in Figure 7.2c) were each changed by substituting different materials (two types of aluminum) for them. Additionally, their thicknesses were varied. Next, the aluminum honeycomb (Figure 7.2d) was replaced with a foam whose properties were developed at Sandia National Laboratories in Albequerque, New Mexico. [Ref. 17]

1. Evaluating Force Dissipation

Evaluation of the force dissipation considered the maximum force applied to an element in the model just above the sole of the boot. This was to simulate the force applied to the tibia.

In addition to peak force, the total impulse (the area under the force versus time curve) was calculated for comparison only, not for its quantitative value. As shown in the verification of the Aberdeen test, Figure 8.1, whereas this model accurately duplicates the peak stress, it does not appear to satisfactorily represent the total impulse. However, it is believed that impulse values obtained by the model can be used in this parametric study

with other values obtained for other variations using the same model. That is to say, although the impulse are not exactly correct, they can be used for relative comparisons.

It should be noted that the goal of varying the components of the shank is to analyze apparent trends that result from using different materials or the same material with a different thickness. The goal is not to find an absolute optimization of the current design. If determined, these trends that may be used later if an optimal design is later sought.

2. Variations in the Shank Base Properties

Two aluminums were considered for replacement of the Type 302 stainless steel currently used. Aluminum 2014-T6 and aluminum 6016-T6 which will be referred to as Al 2014 and Al 6016, respectively, were selected because their properties were significantly different from those found for the stainless steel in Chapter VI as well as there realistic availability and current use in manufacturing. The values used for the different aluminums are listed in Table 8.2.

Table 8.2. Material properties for aluminums. From Ref. [12]

	Density (lb/in^3)	Ultimate Tensile Strength (psi)	Yield Stress (psi)	Modulus of Elasticity (psi x 10^6)
Al 2014	0.101	70	60	10.6
Al 6016	0.098	43	38	10.0

Using type 302 stainless steel that was 28% thinner (0.045 in) produced no change in the maximum force. However, using the same material two times as thick as is currently used (0.125 in) significantly reduced the maximum force to 5562 lbs (a reduction of 19%). This thicker base similarly reduced the total impulse to 4.04 lb-msec. (The impulse for the current design had a value of 4.82 lb-msec.) This is a 16% reduction in impulse. Results of these tests are given in Table 8.3.

Table 8.3. Variations of the shank base.

Base Material	Base Thickness (in)	Top Material	Top Thickness (in)	Max Force (lbs)	% of Current Force
Steel	0.0450	Steel	0.03125	6903	100
Steel	0.1250	"	"	5562	81
Al 6061	0.0550	"	"	6876	100
Al 6061	0.0625	"	"	6921	101
Al 6061	0.1250	"	"	6885	100
Al 2014	0.0625	"	"	6930	101
Al 2014	0.1250	"	"	6804	99

Using both Al 2014 and Al 6016 at varying thicknesses produced essentially no change in maximum force. Using these aluminums at the same thickness as the current steel produced maximum forces at levels of 6930 lbs and 6921 lbs for Al 2014 and Al 6016, respectively. Each approximately 101% of the current design.

3. Variations in the Shank Top Properties

Using the same two aluminums as were used in the base variations, the shank's top was varied in a similar fashion. First, the current material's thickness was varied. Then, each aluminum was used in lieu of the steel at varying thicknesses. Results of these tests are given in Table 8.4.

Decreasing the current thickness of the steel, again, had no significant impact on the maximum force. However, as was found when the base steel was made two times as thick, the max force and the total impulse were reduced. This time the reduction was not near as severe; the reductions of the maximum force and the impulse were each only reduced 3% to 6651 lbs and 4.69 lb-msec, respectively.

Table 8.4. Variations of the shank top.

Base Material	Base Thickness (in)	Top Material	Top Thickness (in)	Max Force (lbs)	% of Current Force
Steel	0.0625	Steel	0.02500	6921	101
"	"	Steel	0.06250	6651	97
"	"	Al 6061	0.02500	692	101
"	"	Al 6061	0.03125	7020	102
"	"	Al 6061	0.06250	7047	102
"	"	Al 2014	0.03125	7020	102

4. Variations in the Aluminum Honeycomb

To analyze the impact of using a material other than aluminum honeycomb to fill the shank, a foam was utilized. The foam selected was Stathane 4802W Rigid Polyurethane Foam

developed at Sandia Labs. (This foam will be to type 4802W foam in this report.) The material properties for this foam were gathered from a force versus strain curve provided by Sandia Labs for this foam whose density was only 1.43×10^{-3} lb/in^3. Attempts to test additional types of foams resulted in errors being generated by our finite element processor (DYNA-3D). So our analysis was limited to studying only one type of foam to replace the aluminum honeycomb. In fact, we were unable to use the type 4802W foam using the boot's current components at their current thicknesses. However, we were able to use this foam in later studies involving variations of both the shank base and shank top. These results will be discussed later in this chapter.

5. Variations in the Base and Top

Utilizing the results previously discussed, we then tested combinations of thicknesses of both the base and the top. Since the utilization of a steel base produced such a marked reduction in maximum force while the other materials had minimal impact (see previous discussion), it was decided to use steel as a base for this phase. Varying thicknesses of the steel base were sampled with varying thicknesses of all three materials as the top of the shank. Results of these tests are given in Table 8.5.

While almost all of the combinations tested produced a reduction in maximum force, this force was minimized when the base steel was three times its current thickness (0.1875 in) and the top was two times its current thickness (0.0625

in). The maximum force was reduced by 15% of the current design to 5886 lbs. The total impulse associated with these thicker dimensions was 26% lower than the impulse generated by the current design.

Table 8.5. Variations of the shank base and top.

Base Material	Base Thickness (in)	Top Material	Top Thickness (in)	Max Force (lbs)	% of Current Force	% of Current Impulse
Steel	0.1250	Al 2014	0.0625	6273	91	88
Steel	0.1250	Al 6061	0.0625	6147	89	89
Steel	0.1250	Steel	0.0625	7281	106	102
Steel	0.1500	Al 6061	0.0625	6003	87	84
Steel	0.1500	Steel	0.0625	6039	88	80
Steel	0.1875	Steel	0.0625	5886	85	74

6. Variations in the Base, Top, and Fill Material

As previously discussed, type 4802W foam was not able to be used for the current thicknesses due to software limitations. However, we were able to use this foam when the dimensions of the shank's components were altered. Results of these tests are given in Table 8.6.

Table 8.6 Varying the shank base and shank top using foam.

Base Material	Base Thickness (in)	Top Material	Top Thickness (in)	Max Force (lbs)	% of Current Force	% of Current Impulse
Steel	0.1250	Al 2014	0.0625	6012	87	85
Steel	0.1875	Al 2014	0.0625	5751	83	76
Steel	0.1875	Steel	0.0625	5886	85	73
Steel	0.1500	Al 2014	0.0625	5607	81	81

Unfortunately, the use of Al 6061 as a top material with the foam created software errors, so the scope of this analysis was restricted to use of the foam as a fill material, steel as a base material and varying thicknesses of steel and Al 2014 as a top material.

As seen in Table 8.6, the optimal minimization of peak force applied to the sole of the foot was a combination of 0.15 in thick steel base and an Al 2014 top with a thickness of 0.0625 in. The force was reduce to 5607 lbs(a reduction of 19%). This combination also reduced the total impulse by 19% to a value of 3.90 lb-msec. It was found that this impulse experienced a greater reduction for those samples involving a thicker steel base of 0.1875 in. For this thicker base, the total impulse values for the 0.0625 in thick tops of Al 2014 and steel were reduced by 24% and 27%, respectively. Therefore, the minimum total impulse involving foam was found with a combination of 0.1875 in thick steel base and 0.0625 in thick steel top.

7. Impact of Component Variations on Boot Weight

Given the very nature that these countermine boots will most likely be worn by soldiers while conducting normal operations and countermine operations, the weight and comfort of the boot is critical. Since this study focuses on the analysis of a rigid, inflexible shank, there is little that can addressed regarding comfort except that the

shanks overall length of approximately 5.7 in should allow normal flexure of the forefoot. Weight, however, is an issue that is effected by this analysis.

Each men's size nine countermine boot in its current design weighs 2.38 pounds. The shank in the boot accounts for 16% of this weight (0.37 lbs). Needless to say as the components of the boot are varied in material and thickness the weight also varies. Because the shank only accounts for 16% of the overall boot weight, small changes in thicknesses had relatively little impact on the overall boot weight. Because some of designs discussed previously had a rather large impact on the maximum force and/or total impulse, the weights of these designs were calculated to give some appreciation for the trade-off between blast dissipation and overall weight of the boot. The results of several of these designs are listed in Table 8.7.

As can be seen in Table 8.7, the lightest boot comination is also the combination that results in the lowest level of maximum applied force. The lightest weight design involving aluminum was heavier than a design involving both a steel base and top because of the additional thickness of the base required to keep the maximum force on the tibia low.

Table 8.7 Impact of component variations on boot weight.

Base Material	Thickness (in)	Top Material	Thickness (in)	Fill Material	Max Force* (lbs)	Boot Weight* (lbs)
Steel	0.1250	Steel	0.03125	Honeycomb	5562 (81%)	2.62 (110%)
Steel	0.1875	Steel	0.06250	Honeycomb	5886 (85%)	2.96 (124%)
Steel	0.1500	Al 2014	0.06250	Foam	5607 (81%)	2.66 (112%)
Steel	0.1875	Al 2014	0.06250	Foam	5751 (83%)	2.80 (118%)
Steel	0.1875	Steel	0.06250	Foam	5886 (85%)	2.92 (123%)

* Also indicated are the percentages of the current design's values.

IX. CONCLUSIONS

Four materials from the countermine boots were tested to determine the material properties of each: rubber, aluminum honeycomb, steel, and kevlar. Throughout the testing, ASTM standards were adhered to as much as possible. However, due to the limited dimensions of the available material, it was necessary to scale the ASTM standards for some of the specimens.

The testing conducted on the cylindrically-shaped rubber specimens had very consistent results. Several rubber specimens from two different boots behaved in the same manner and proved have the same compressive properties and same Young's modulus throughout their elastic regions.

Testing on the aluminum honeycomb was conducted in three different directions using specimens from two countermine boots and one countermine overboot. Properties were found to be consistent regardless of the source. The failure strength in the vertical direction proved to be over twenty times stronger than that found in either the longitudinal or transverse directions. Similarly, the average Young's modulus found in the vertical direction was more than fourteen and twenty-eight times stronger than those found in the longitudinal and transverse directions, respectively.

The steel used on the upper portion of the shank was proven to be the same Type 302 Stainless Steel as used on

the bottom of the shank. This was done by a microanalysis of both using Scanning Electron Microscope and an Electron Dispersive X-ray. The lower steel was then tested and proved to have material properties consistent with those expected of a Type 302 Stainless Steel.

The testing of the kevlar was conducted in both transverse and longitudinal directions. The failure strengths of the specimens were found to be the same in either orientation. The Young's moduli were found to be of the same magnitude but were much greater in the longitudinal direction.

The finite element model has proven to be an accurate indicator of peak forces imparted to the lower extremities of the body. This was verified by a comparison with a test conducted by the U.S. Army Aberdeen Test Center. The boot rubber compressed as expected and the shank collapsed to help absorb the energy of the blast. While this model was not found to be an accurate quantitative model for the total impulse, it was a useful tool for an analytical study. This was very helpful in the next stage of this study which not only analyzed peak forces but looked at total impulses as well.

The current boot design was found to dissipate the blast force to 6,885 lbs. This was lower than the critical compressive force in a mid-sized male, 8,070 lbs. However, it must be remembered that for a small female, acceptable forces are much lower. In this case, the values for a

female are below those achieved by any of the designs anlalyzed in this study. However, the goal of this project was to analyze the boot and try to determine design trends, not to optimize the current design to meet any given parameters or thresholds.

Varying the material dimensions produced several observable trends in alternate designs. Variations in the base only dissipated in the maximum force when the steel base thickness was increased. It is expected that further increases will continue to produce lower force levels. Top thickness and material variations had very little impact on the reduction of the force applied to the foot. However, like the base, increasing the steel's thickness proved most advantageous to force reduction.

The variations of the current design's top and bottom materials and thicknesses proved, again, that the use of thicker steel maximizes force dissipation. For all of these combinations addressed thus far, the total impulse was reduced proportionally with maximum force.

Varying the top and bottom with the foam produced an interesting result. That is, when foam was utilized the use of Al 2014 as a top material actually produced lower force levels than the use of steel with the same thickness. In fact, an Al 2014 top produced the lowest force when it was not combined with the thickest steel base. Total impulse, however, followed the same trend as earlier tests; as the steel base became thicker, the total impulse was reduced.

In short, the reduction of total impulse can most easily be achieved through the use of a thicker steel base. However, there are combinations involving varying thicknesses of an aluminum top and foam that will produce the minimum force applied to the foot.

As was seen in Table 8.7, there are variations that can reduce the maximum force by as much as 19% while only increasing the boot weight 10-12%. Depending on the price, availability, and the ease of manufacturing the shank with steel, aluminum, aluminum honeycomb, and foam, there is are a variety of options from which to chose.

The Finite Element Model, while in its most preliminary form, has given some insight into the nature of the explosion and the forces involved. The time history plots of the force fields shown in this section would seem to suggest damage and injuries consistent with land mine victims. All of the materials of the boot undergo some amount of permanent deformation and failure.

X. RECOMMENDATIONS

If a decision must be made solely on the results of this study, it is recommended that the the current steel base thickness be increased two-fold to a thickness of 0.125 in. As discussed earlier, this will reduce the load on the tibia by 19% with only a 10% increase in boot weight. This should also simply the changes required in the machining and manufacturing processes of the boot and its components.

If an absolute optimization for the current design is sought, it is recommended that the current finite element model be modified to account for ankle mobility and soft tissue accountability. This tissue may provide additional and beneficial damping to the system. However, accounting for the destruction of this tissue and accompanying blood loss will prove difficult at best. It is also considered essential to validate this model with carefully conceived and executed live fire testing on cadaver limbs.

APPENDIX A. MICROANALYSIS OF THE STEEL SHANK

In order to most accurately determine the type of steel used as a shell for the aluminum honeycomb filled shank, a Scanning Electron Microscope (SEM) was used in conjunction with an Energy-Dispersive X-ray (EDX) microanalysis. The result of this analysis was that the steel used for both the thin top and thicker wedge-shaped base are both Type 302 Stainless Steel.

The SEM is a more recent innovation in electron microscopy and has proved to be an extremely useful investigative tool. For this analysis, unprepared samples of the steel shank cover were placed in the SEM. (As long as the samples are electrically conductive, no coating or other sample preparation is necessary.) The surface of each sample was scanned with an electron beam. The electrons reflected from the surface are collected and displayed on a cathode ray tube. The features of the surface of the sample appear on the tube (like looking at a TV screen). A complete description of the process used for the SEM is given in ASTM E986-92, [Ref. 18] Standard Practice for Scanning Electron Microscope Performance Characterization.

The EDX is attached to the SEM as an accessory and allows for qualitative and quantitative analyses of the elemental composition of the small section of each sample being scanned by the electron beam. A brief explanation of

how each element is identified by the EDX follows: When the electron beam strikes an element in the sample, electrons are ejected from inner atomic shells to outer shells resulting in ions in the excited state. When the element relaxes, these ions return to their original shells returning the element to a normal ground state. The most likely case involves a series of transformations in which electrons drop from one shell level to fill a vacancy in an inner shell. The drop from each shell level gives off an amount of energy equal the energy between the two shell levels. The energy is given up in the form of electromagnetic radiation. Knowing the shell level energies of each element, the EDX is able to measure the energy discharged by the sample's atoms and identify which elements are present. The EDX can then display the amount of any elements present in the sample to the user in the form of weight percent. An in-depth description of the procedure used in the EDX analysis is given in ASTM E-1508-93a, [Ref. 19] Standard Guide for Quantitative Analysis by Energy-Dispersive Spectroscopy.

One limitation of the EDX arises when elements with similar atomic numbers are present. The result can often be that the two elements will appear in the same "peak" on the screen of the EDX. This is a result in the similar amounts of energy between shell levels. In order to separate the two elements, a method of Gaussian deconvolution is used to separate the overlapping peaks.

An EDX microanalysis of the two type of steel samples was used along with the ASM Source Book on Stainless Steels [Ref. 20] to identify the type of steel used in the shank.

Initial analysis proved to be accurate enough to declare the thin top of the shank and the thicker bottom of the shank were made of a common iron-chromium-nickel steel; that is, a type 300 series steel. Both samples possessed a Chromium content within 1.8 percent of each other and Nickel composition within 1.1 percent. However, in order to most accurately determine the AISI type of steel, both of the samples were reanalyzed. This analysis requested that the amount of Manganese be determined and utilized Gaussian deconvolution. This was done because the atomic numbers for Chromium, Manganese, Iron, and Nickel are 24, 25, 26, and 28, respectively. The results indicated weight percentages as follows: 71% Iron, 19% Chromium, 8% Nickel, and 2% Manganese. These values were then compared to the AISI standards for different types of steel and it was found that they were consistent with AISI Type 302 stainless steel [Ref. 14]. Results are indicated in Table A.1.

Table A.1 Comparison of elemental content.

	% Cr	% Ni	% Mn
AISI Type 302	17-19	8-10	2.00
Thin Sample	18.96	7.83	1.90
Thick Sample	20.67	7.62	1.79

APPENDIX B. STRESS VS STRAIN CURVES OF RUBBER SPECIMENS

Figure B.1 compares stress vs strain curves for three rubber samples from the same boot (Boot #1).

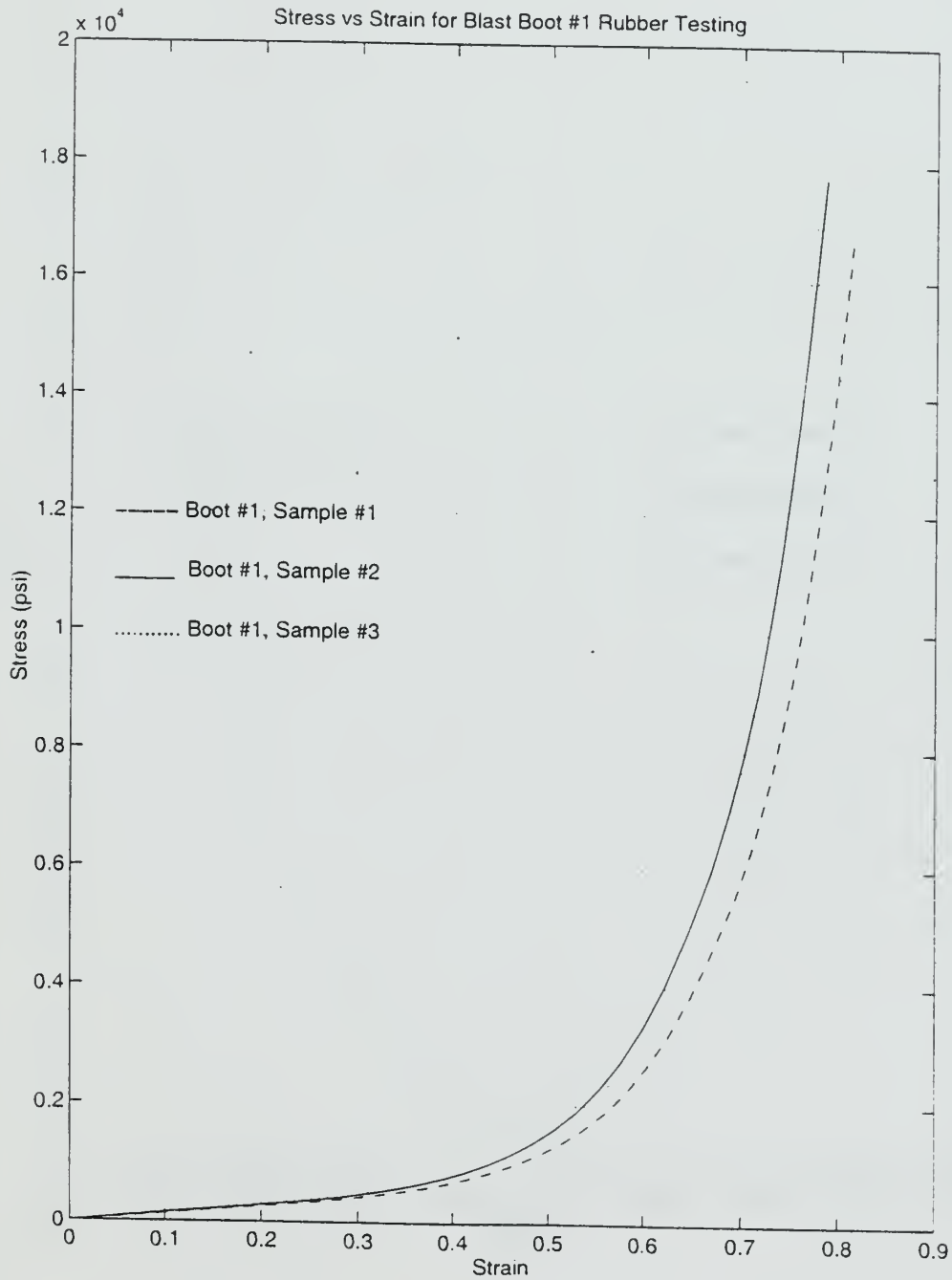

Figure B.1

Figure B.2 compares stress vs strain curves for three rubber samples from the same boot (Boot #2).

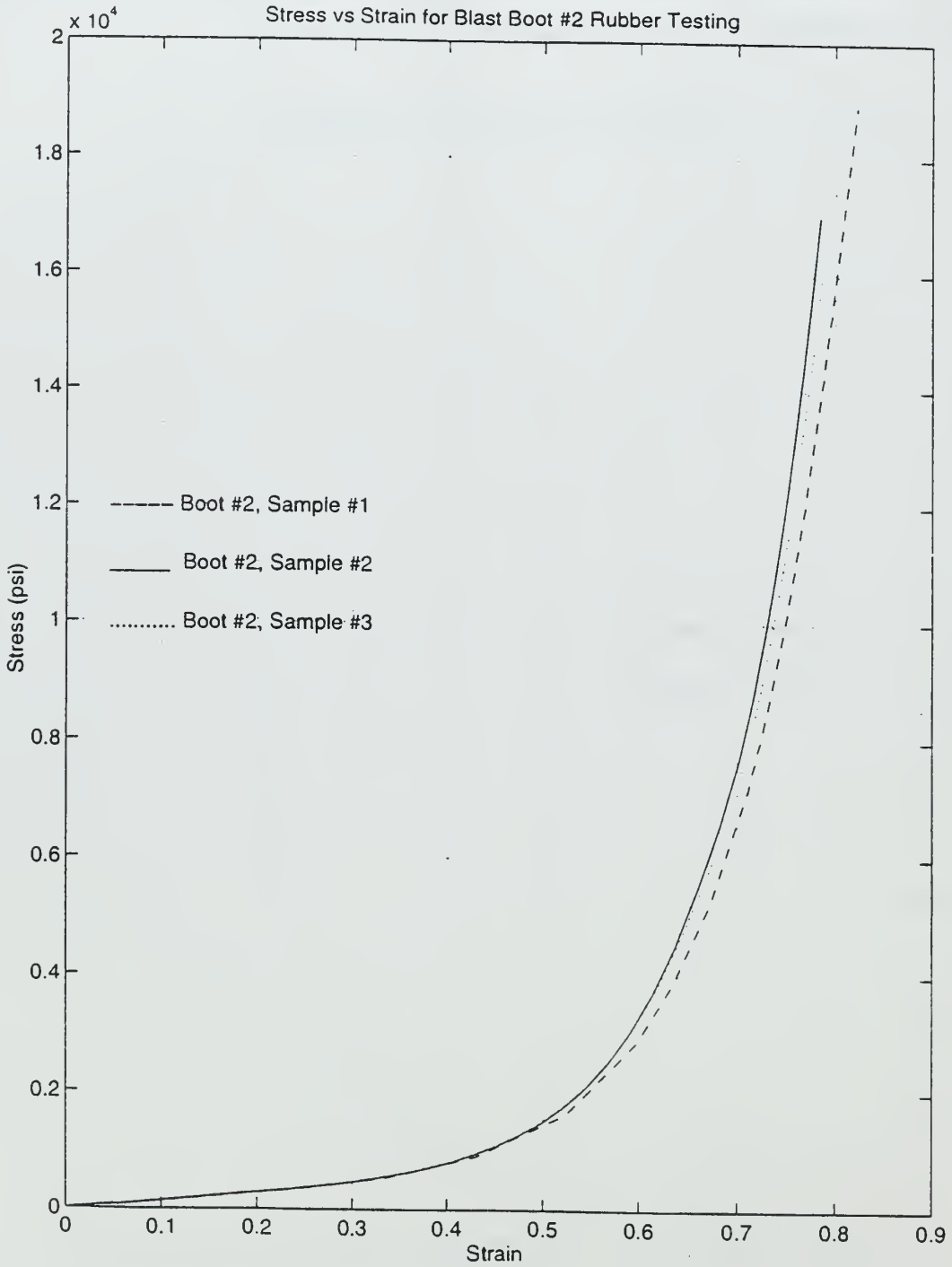

Figure B.2

Figure B.3 compares stress vs strain curves for two rubber samples (Samples #1) from the two different boots.

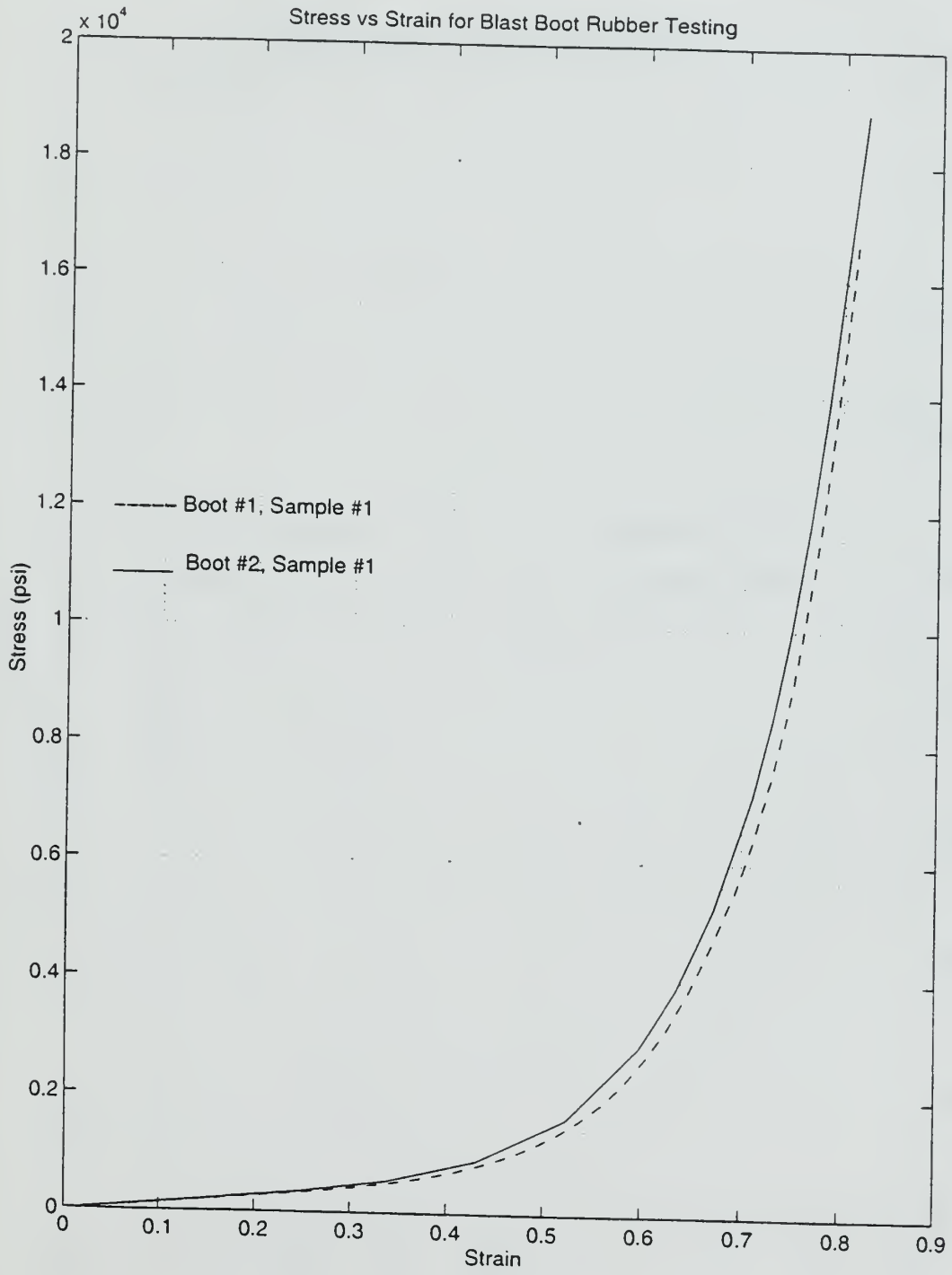

Figure B.3

Figure B.4 compares stress vs strain curves for two rubber samples (Samples #2) from two different boots.

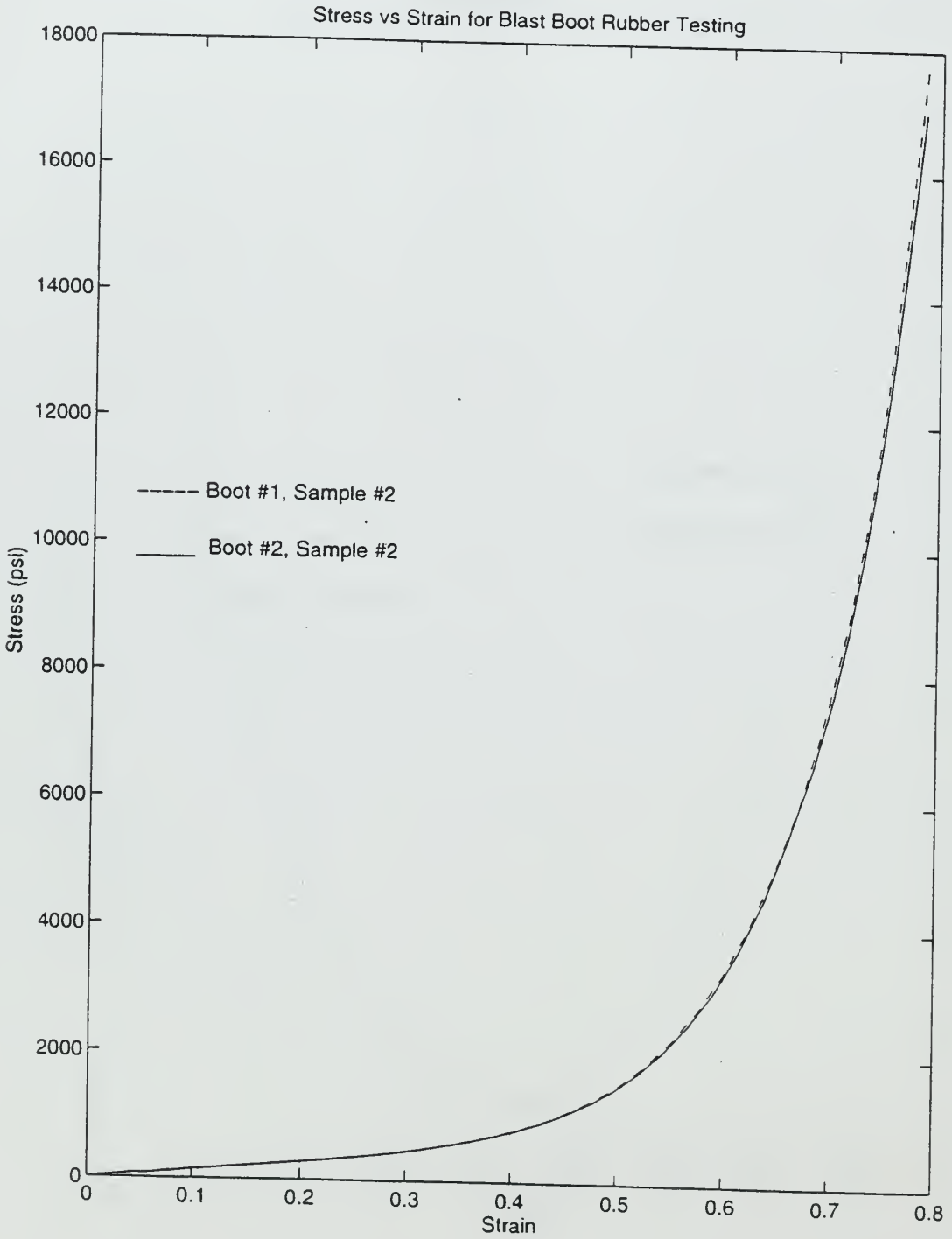

Figure B.4

Figure B.5 compares stress vs strain curves for two rubber samples (Samples #3) from two different boots.

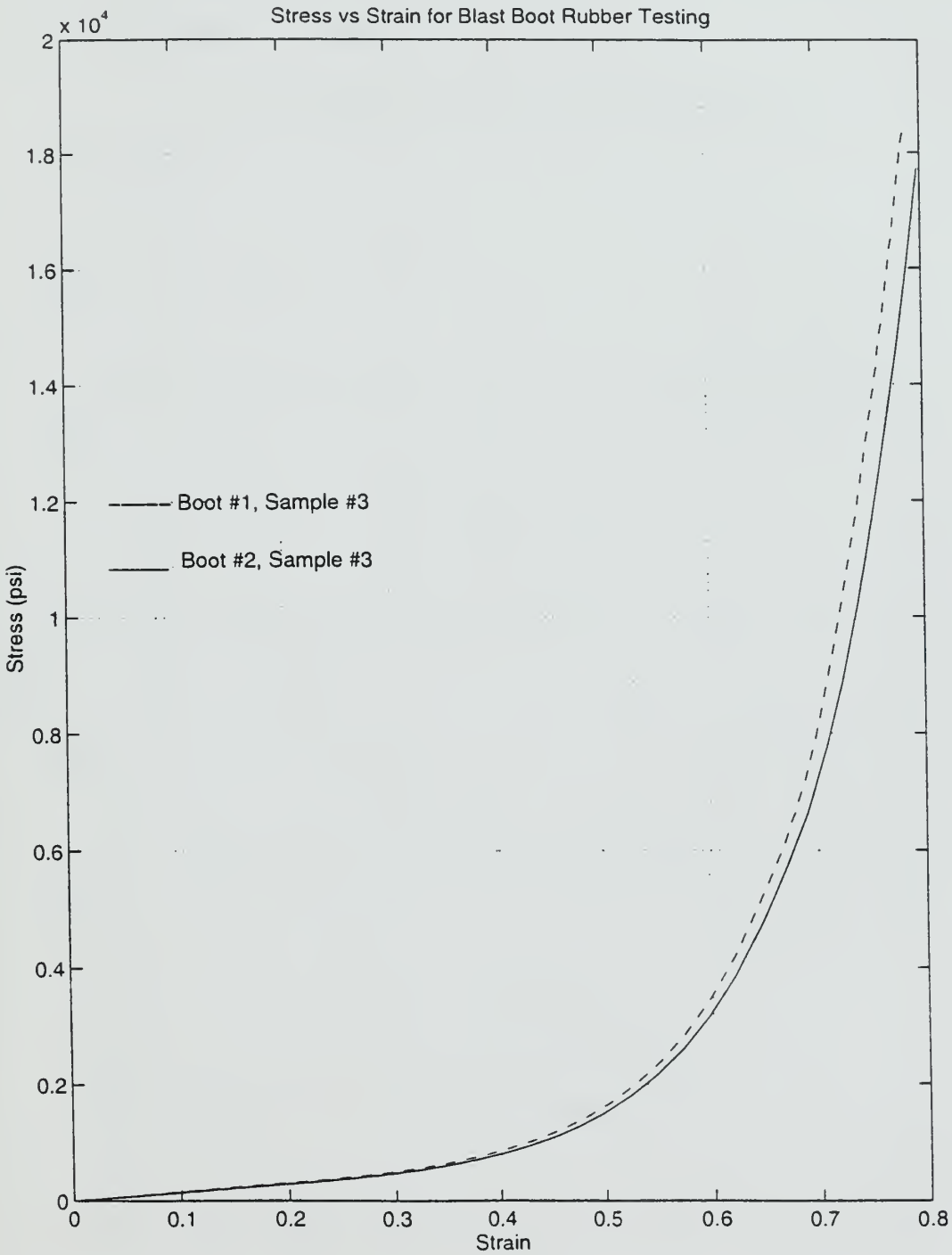

Figure B.5

APPENDIX C. STRESS VS STRAIN CURVES OF HONEYCOMB SPECIMENS

Figure C.1 compares stress vs strain curves for three honeycomb samples compressed in the downward direction shows consistent behavior for all three specimens.

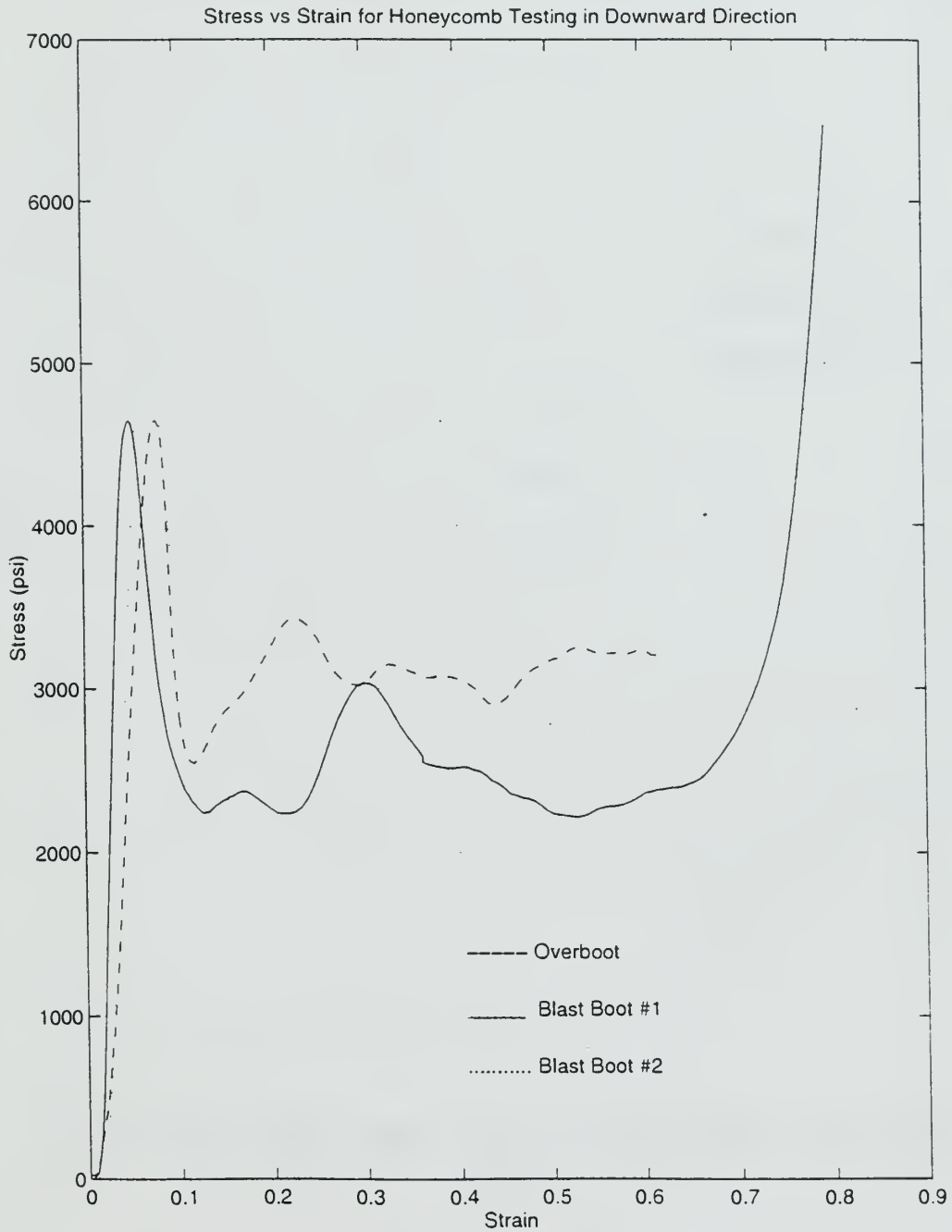

Figure C.1

Figure C.2 compares stress vs strain curves for three honeycomb samples compressed in the longitudinal direction shows consistent behavior for all three specimens.

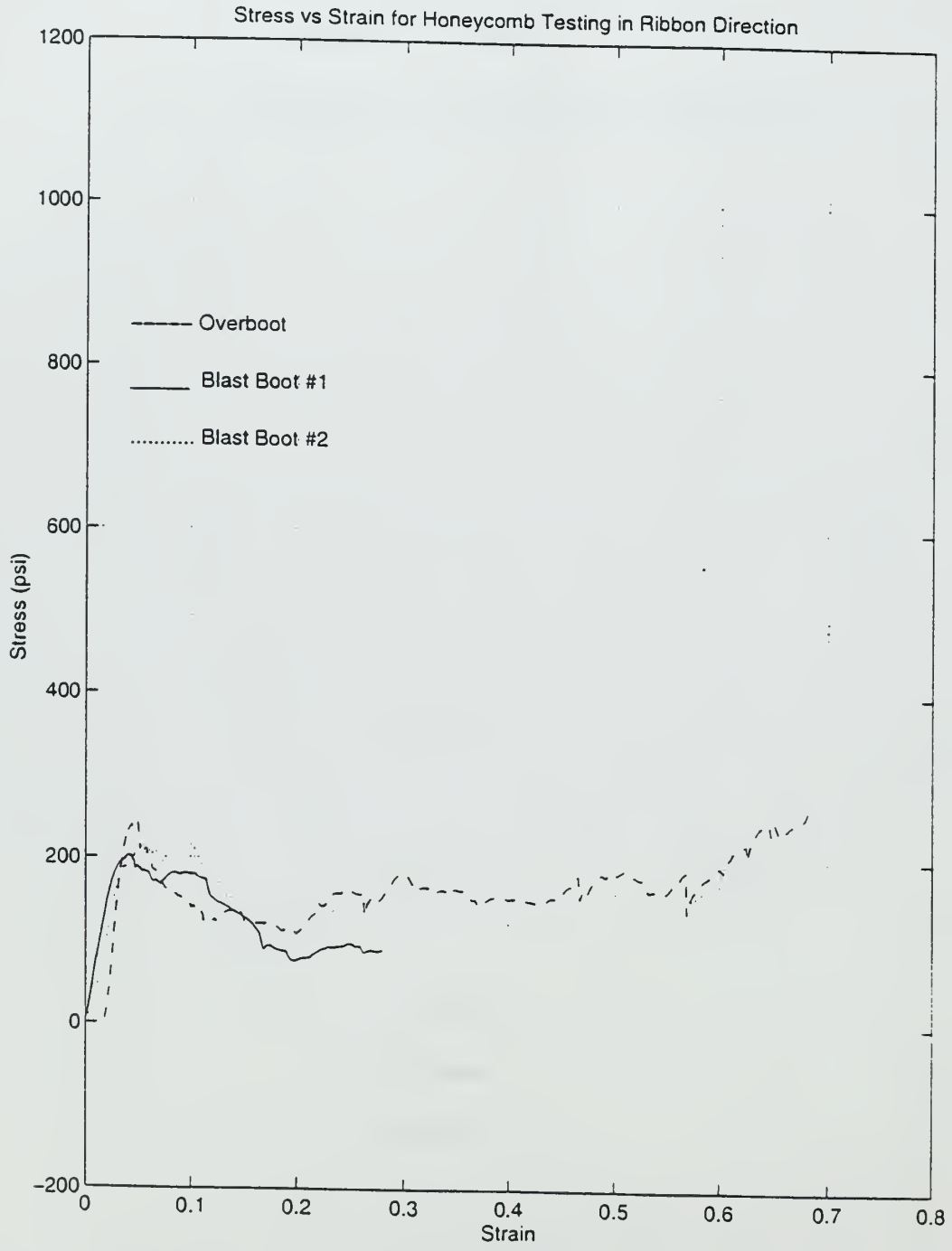

Figure C.2

Figure C.3 compares stress vs strain curves for three honeycomb samples compressed in the transverse direction shows very similar behavior throughout the compression.

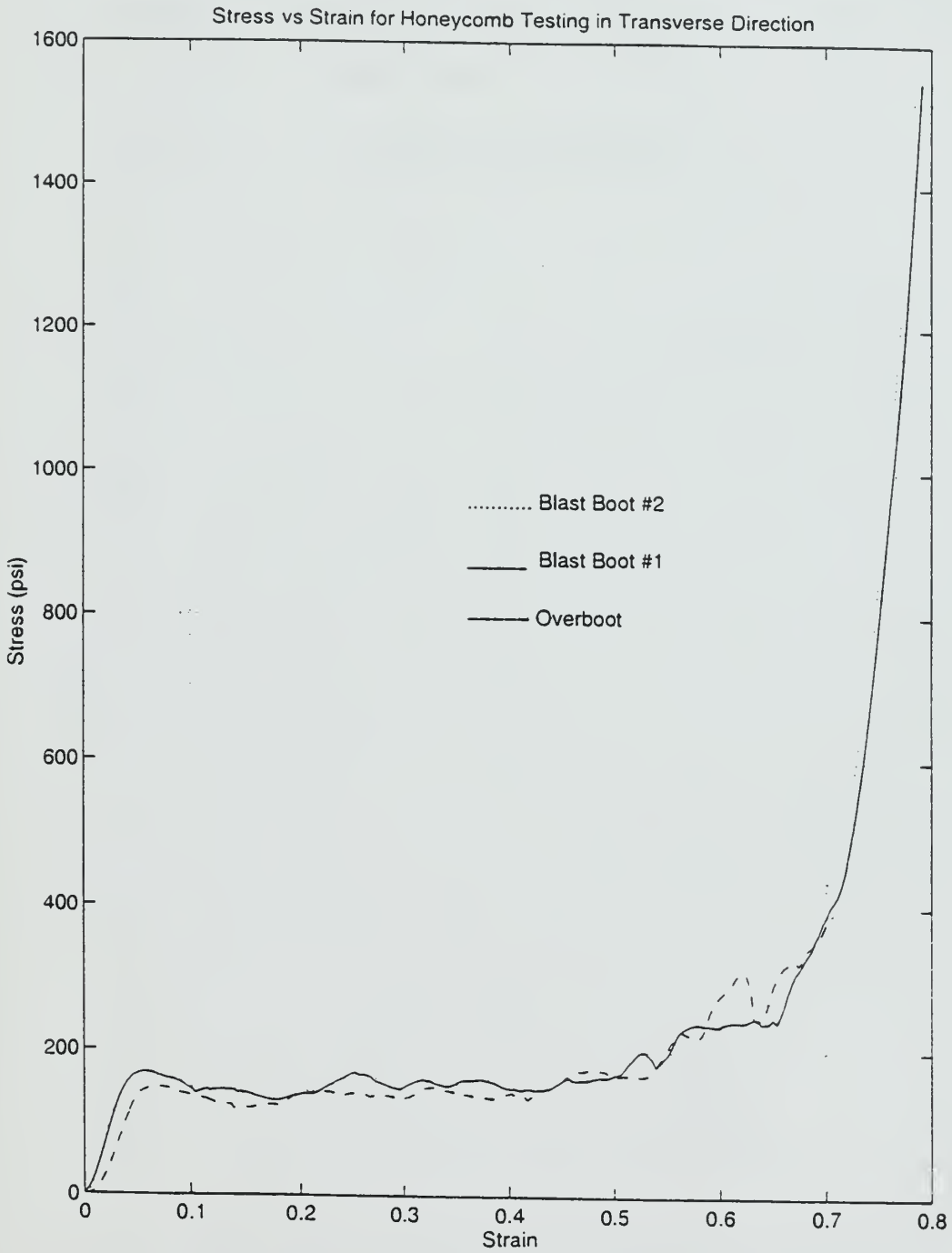

Figure C.3

APPENDIX D. STRESS VS STRAIN CURVES OF STEEL SPECIMENS

Figure D.1 compares stress vs strain curves for three steel samples samples shows the closeness of yield strengths and very similar Young's moduli for Samples 2 and 3.

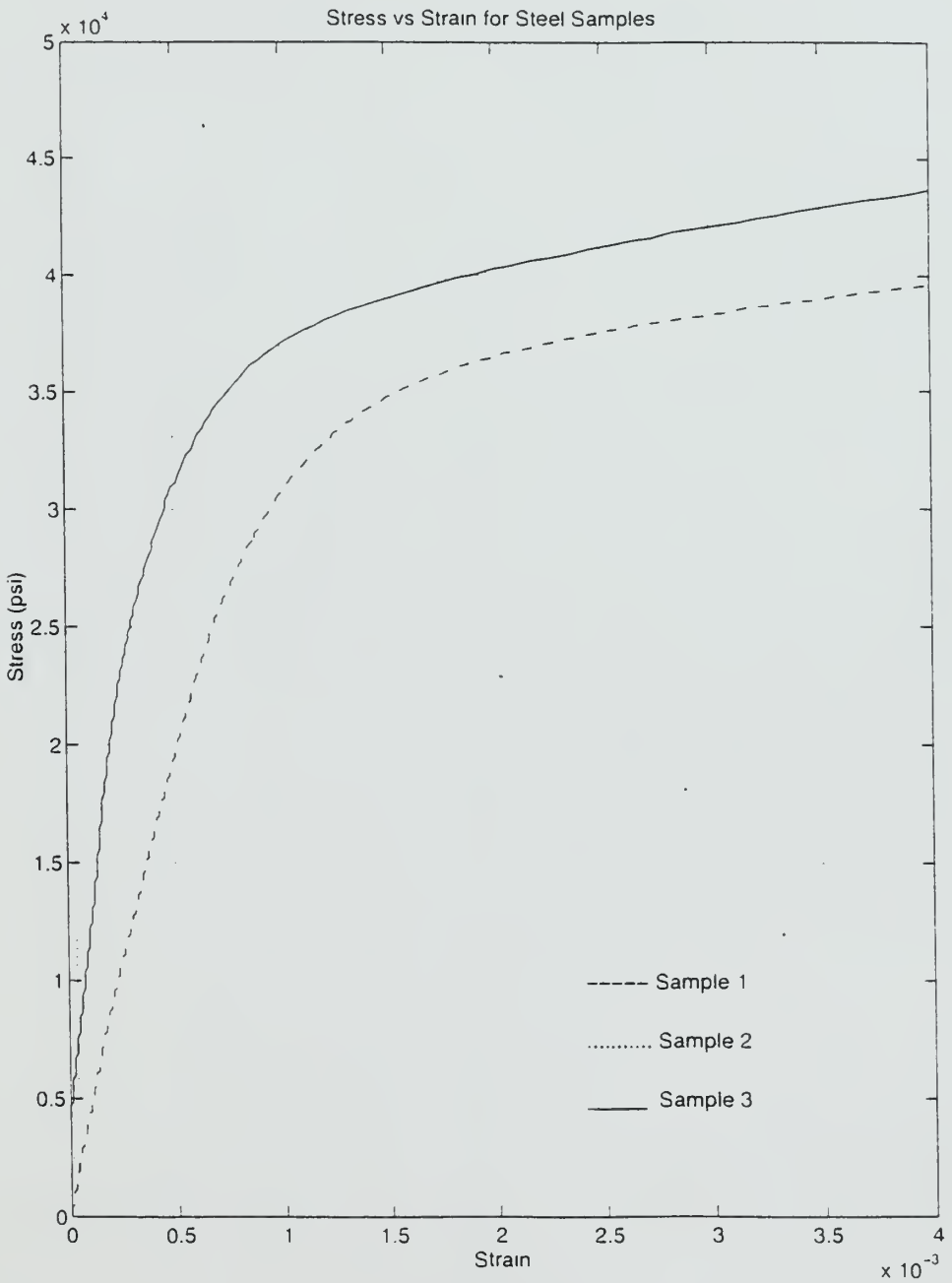

Figure D.1

APPENDIX E. STRESS VS STRAIN CURVES OF KEVLAR SPECIMENS

Figure E.1 compares stress vs strain curves for two of the transverse kevlar samples shows very close Young's moduli and failure strengths.

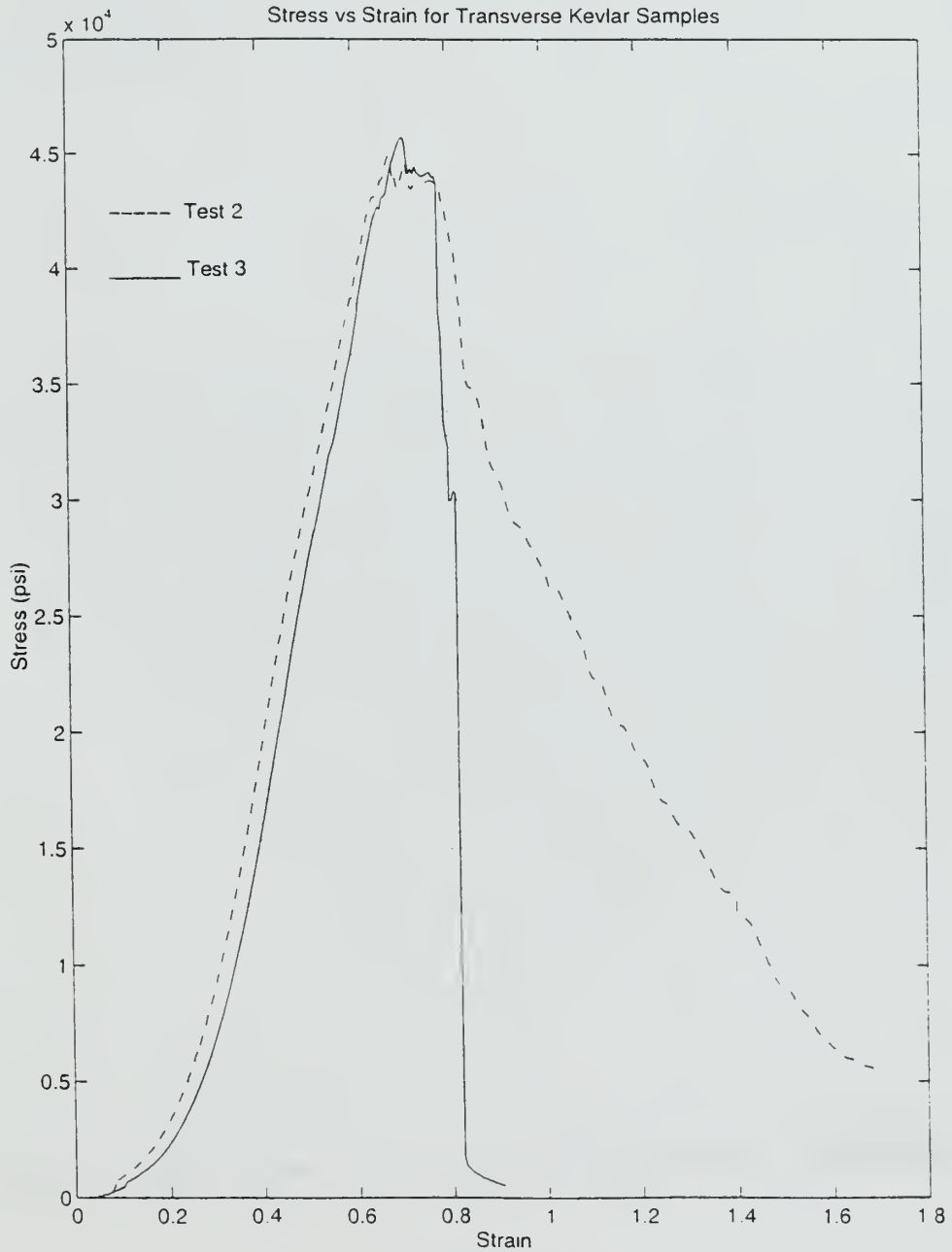

Figure E.1

Figure E.2 compares stress vs strain curves for two longitudinal kevlar samples shows relatively close failure strengths.

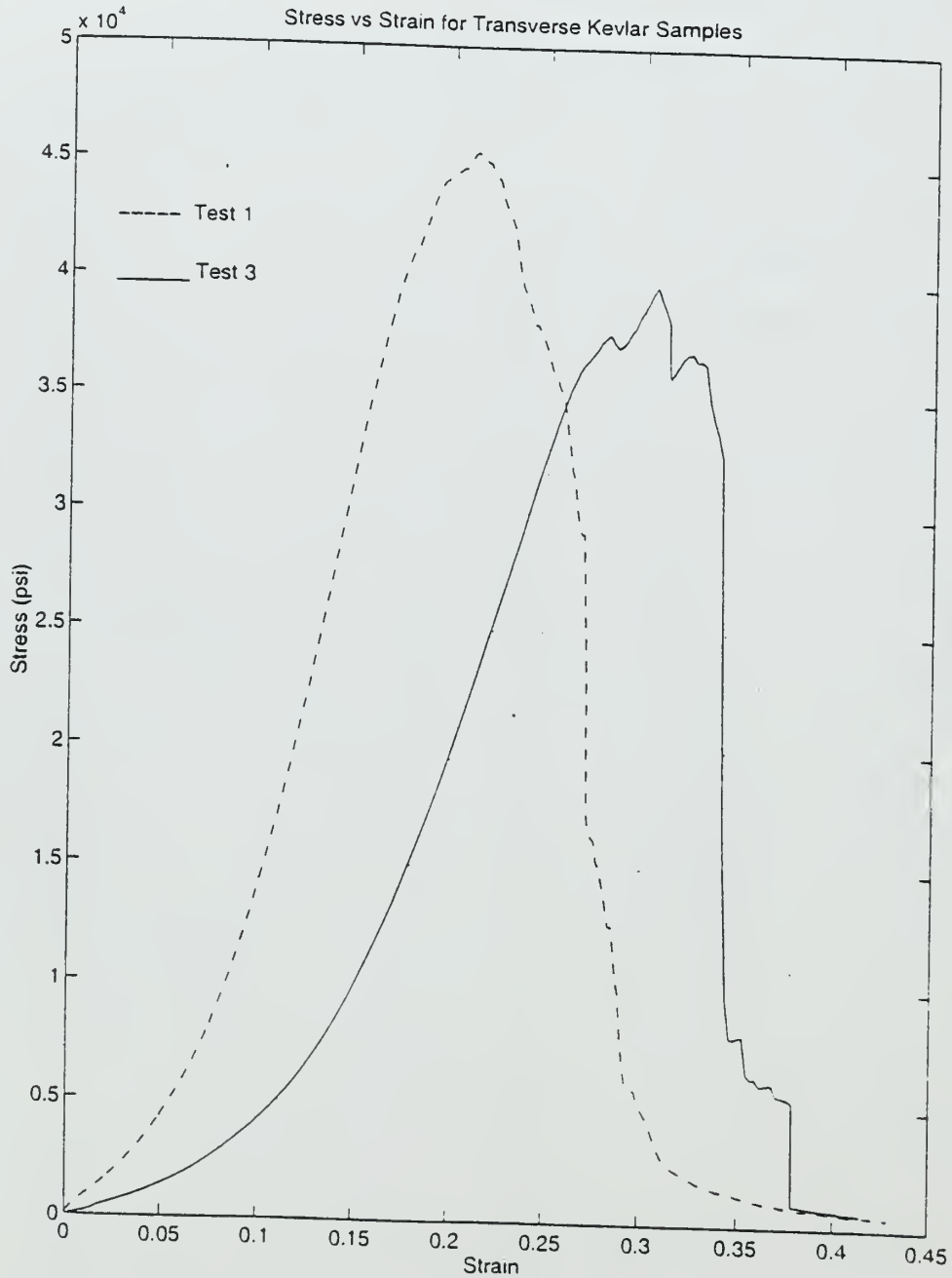

Figure E.2

APPENDIX F. ELEMENT LOCATIONS IN THE FINITE ELEMENT MODEL

Figure F.1 shows a cross-sectional view of the entire finite element model with element numbers identified.

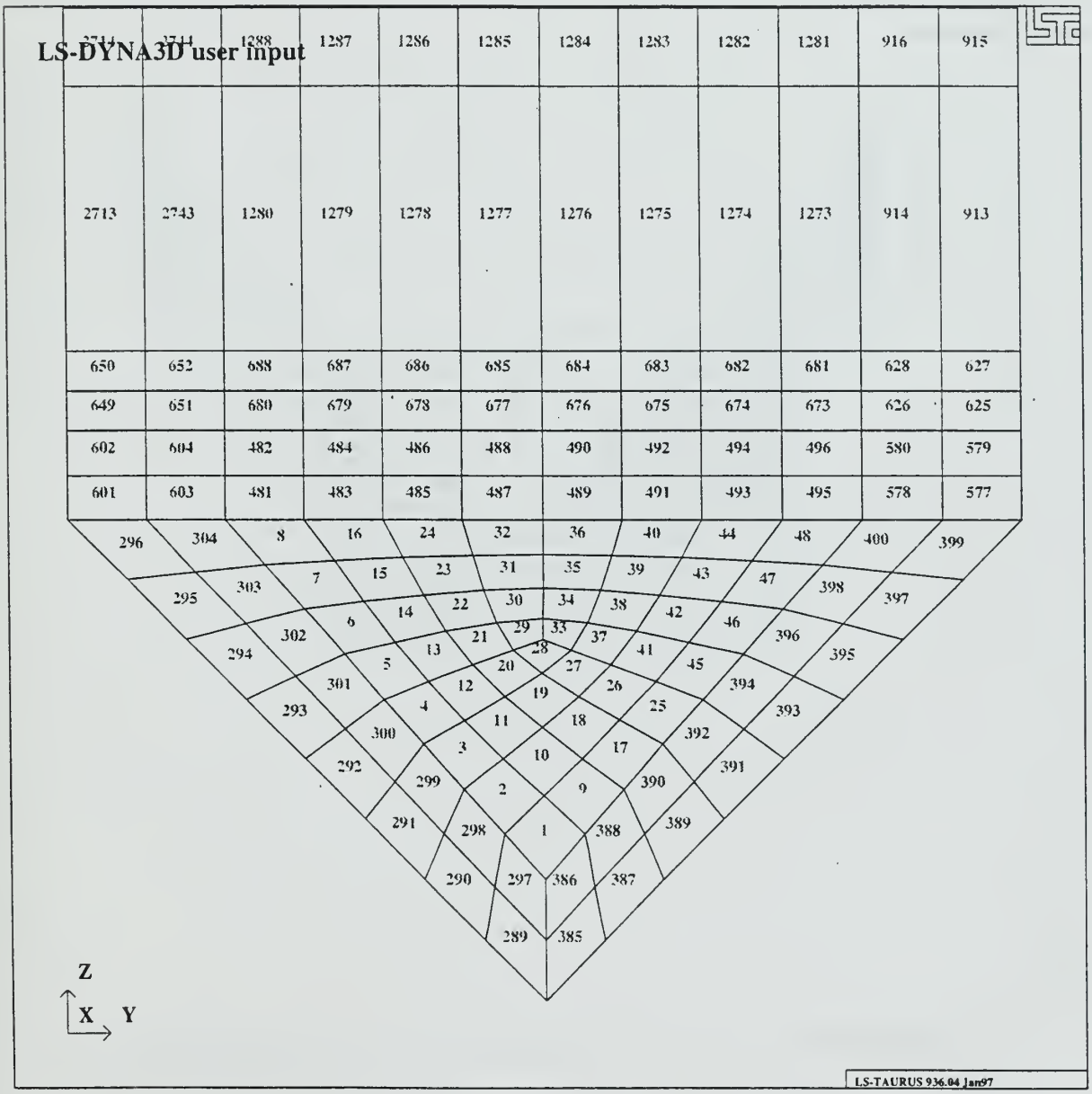

Figure F.1

Figure F.2 shows a side view of the entire finite element model with element numbers identified.

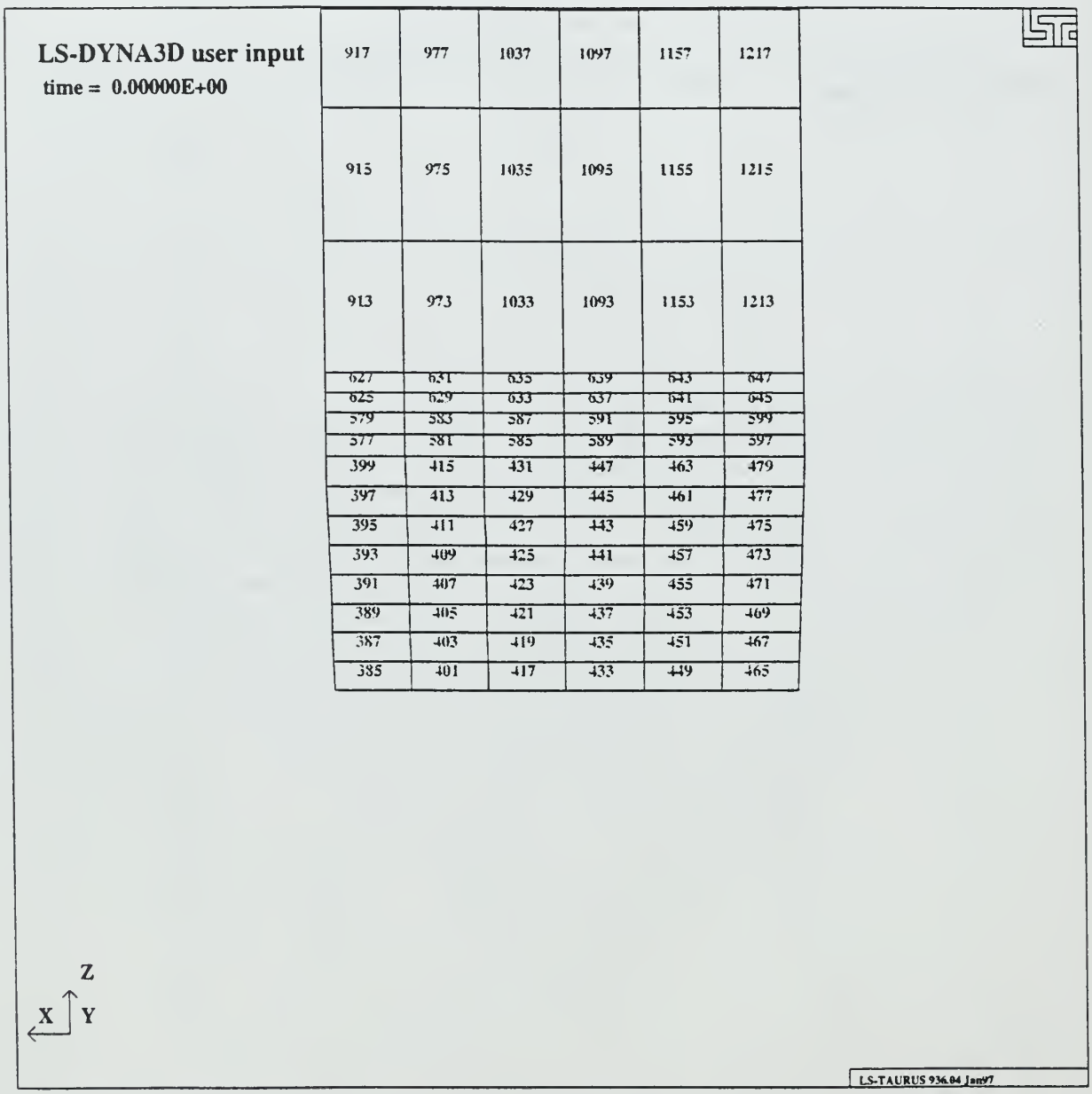

Figure F.2

Figure F.3 shows the rubber model with element numbers identified.

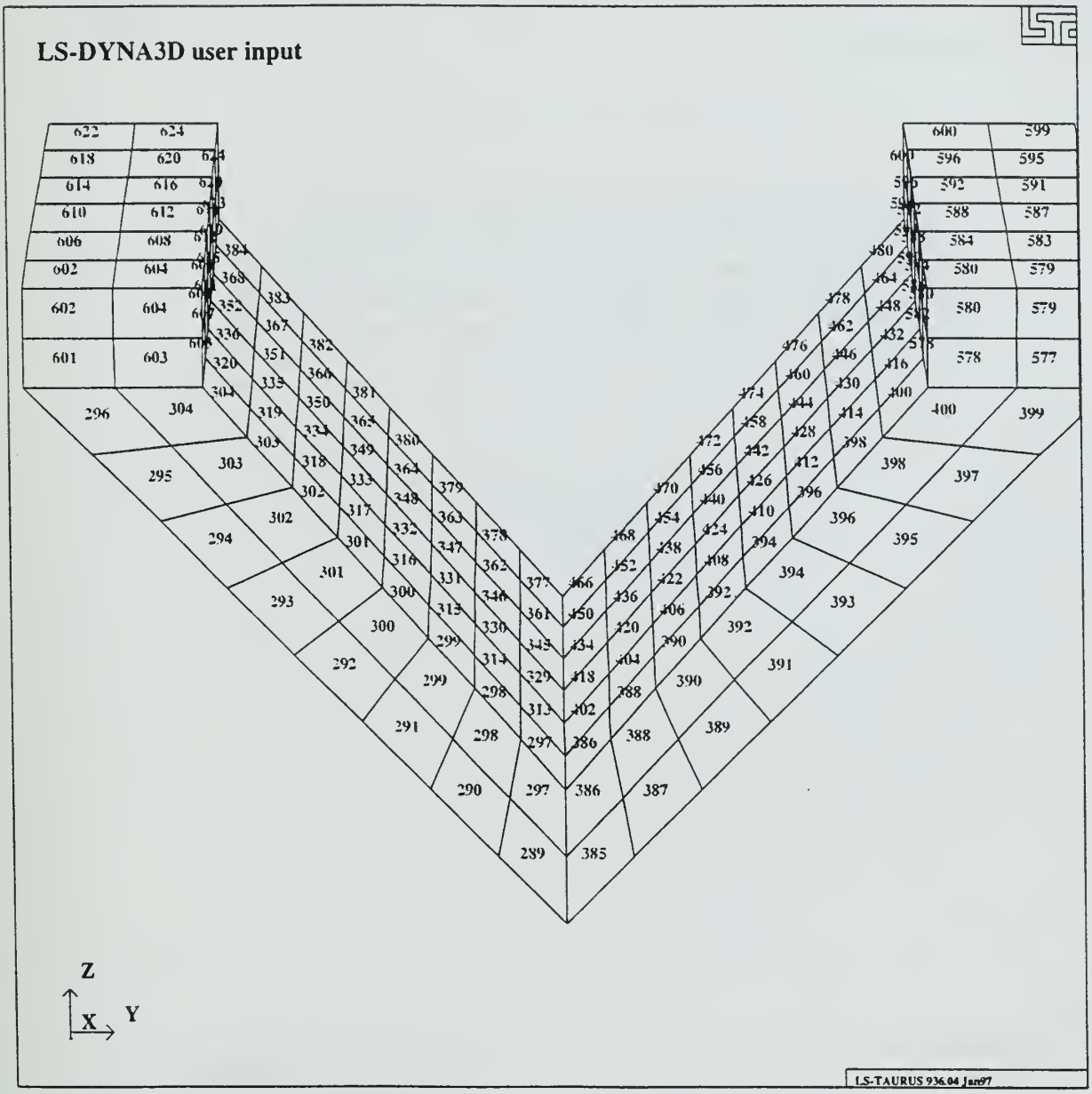

Figure F.3

Figure F.4 shows the honeycomb model with element numbers identified.

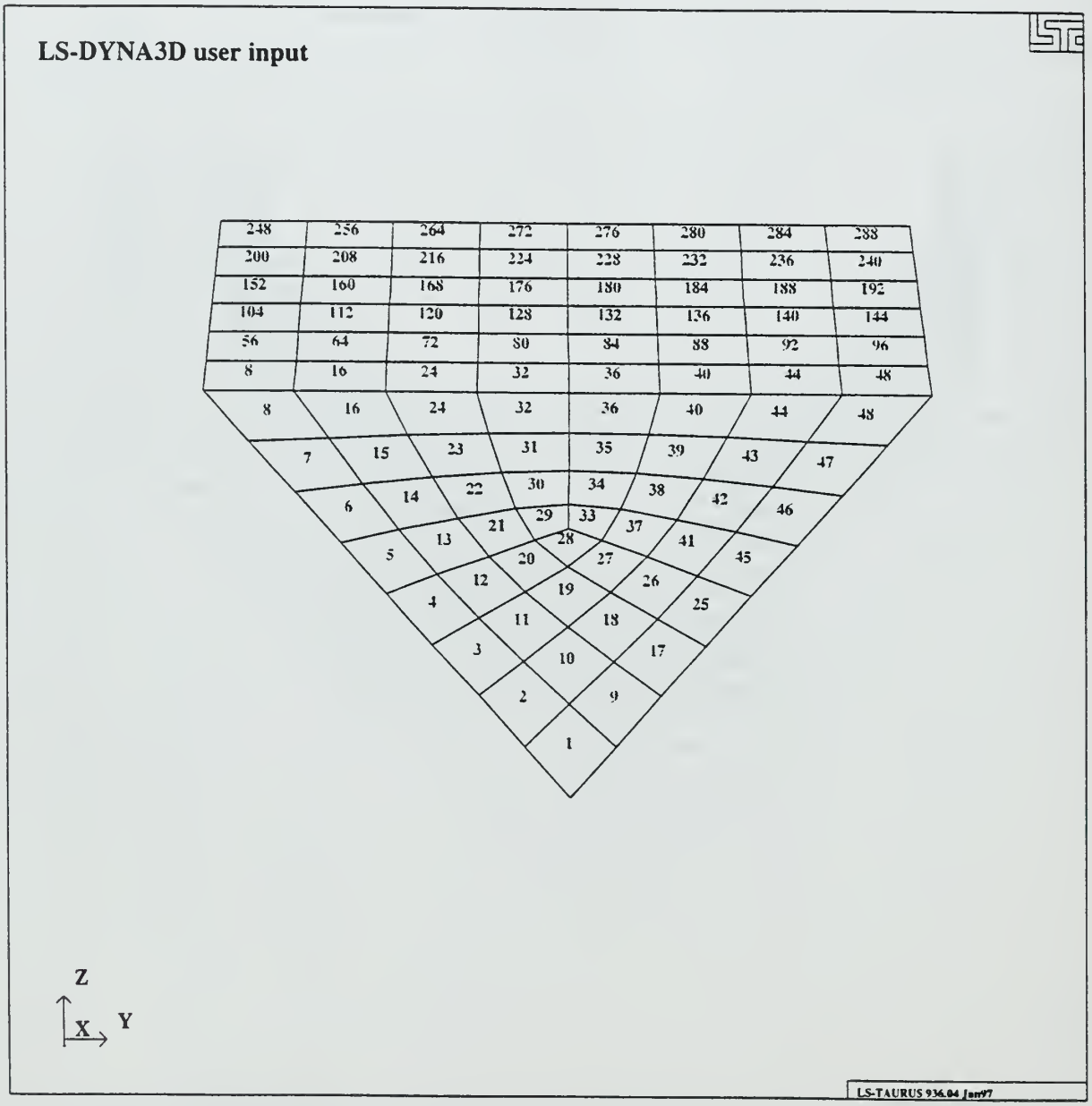

Figure F.4

Figure F.5 shows the stainless steel shell model with element numbers identified.

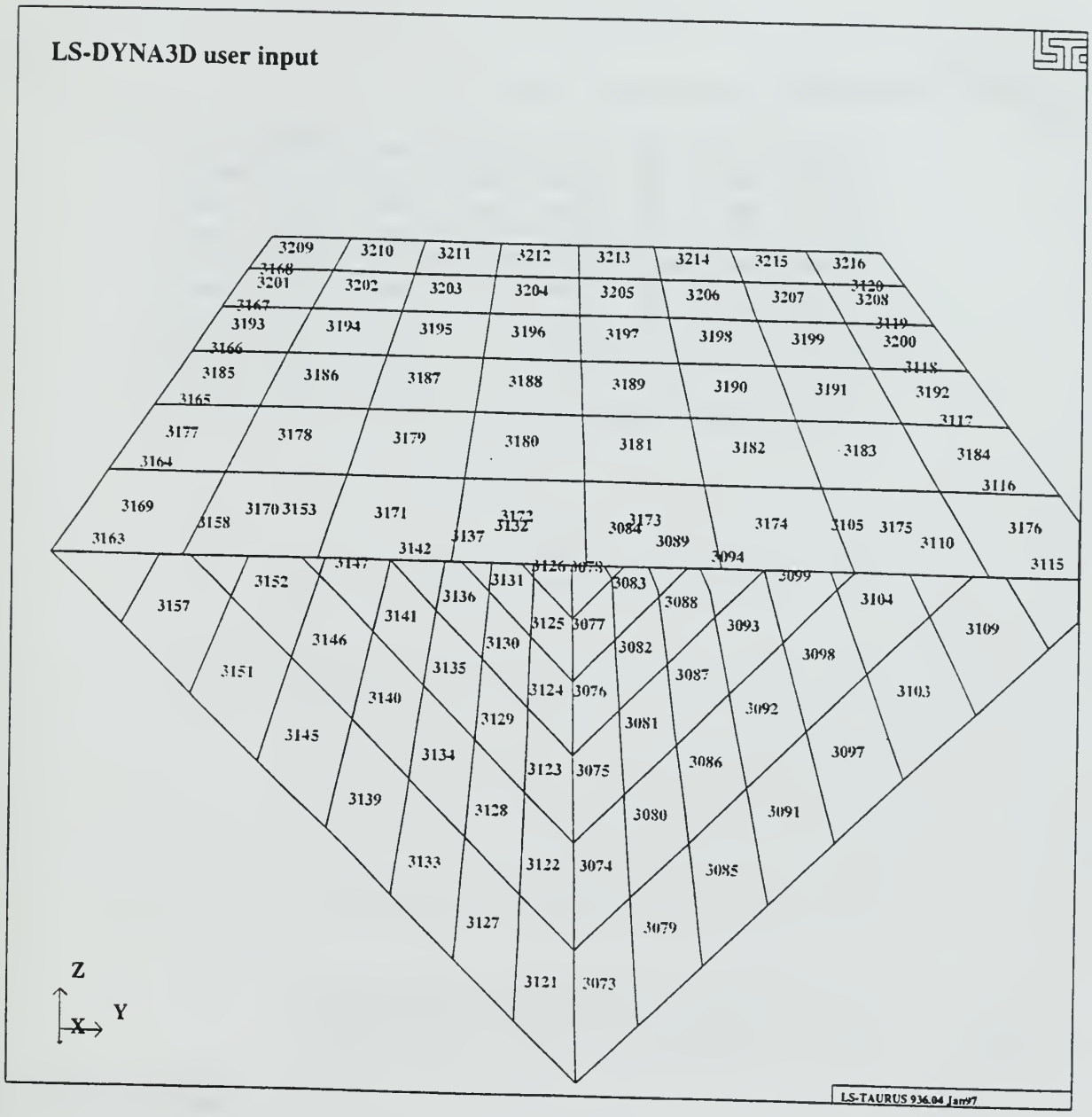

Figure F.5

Figure F.6 shows the kevlar liner model with element numbers identified.

Figure F.6

Figure F.7 shows the lower portion of the bone model with element numbers identified.

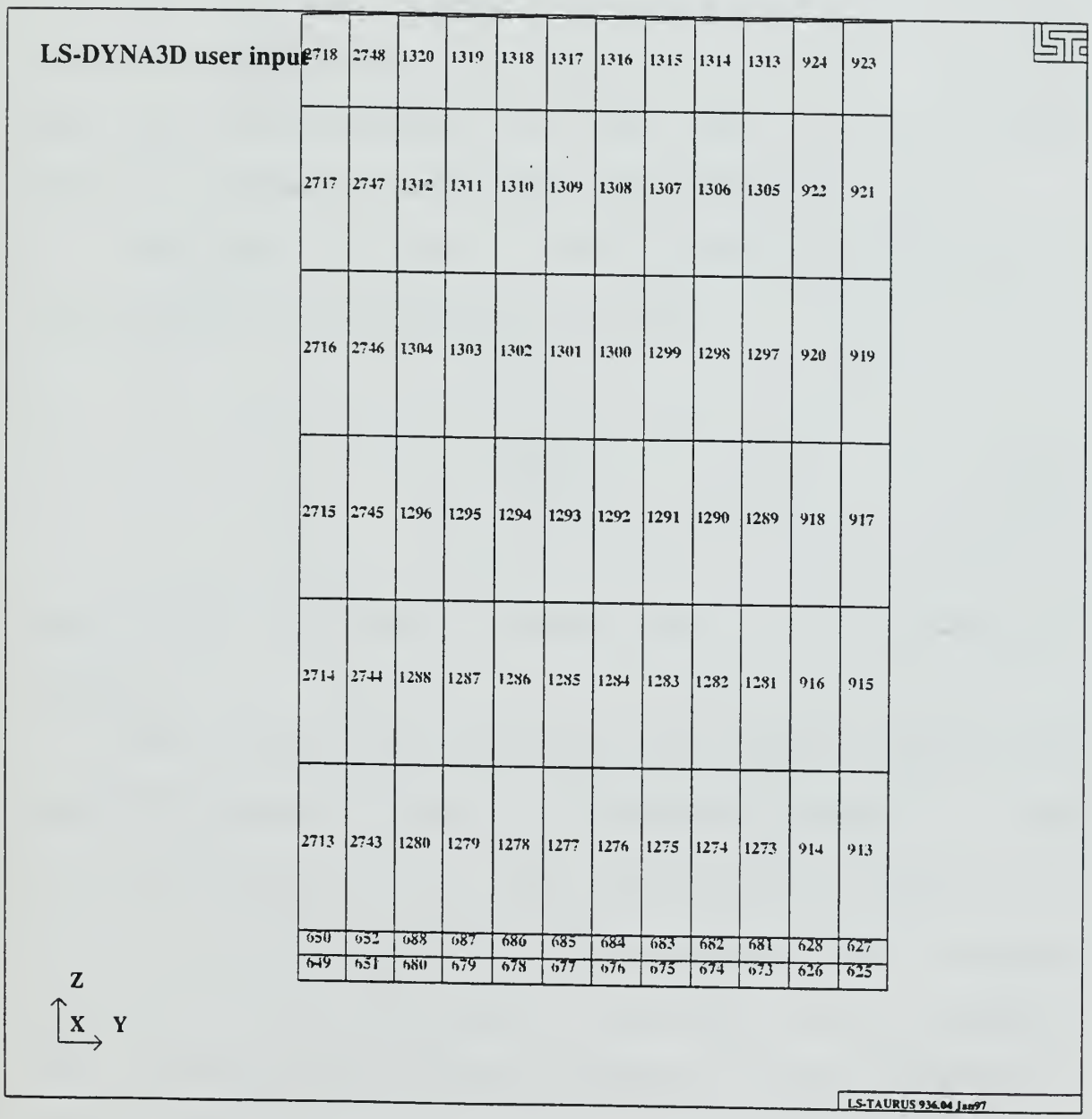

Figure F.7

APPENDIX G. SHOCK WAVE PROPOGATION

It is beyond the scope of this project to fully discuss or explain shock-wave propogation. However, a fundamental understanding of how shock waves propogate through materials and role that the impedence of the materials plays will assist in understanding the results of this work. That is, why the shank dissipates the blast wave differently when different materials i.e., steel or aluminum, are used.

The speed at which a shock wave passes through a material can be calculated as follows:

$$c = \sqrt{\frac{E}{\rho}} \tag{G.1}$$

where E is the Young's modulus and ρ is the material density.

When a shock wave encounters an inerface between two materials normally, there is a transmitted pressure, σ_t, and reflected pressure, σ_r. The characteristic impedence is defined as ρc for each of the materials. This impedence relates to stress attenuation in simple layered systems. The transmitted and reflected stresses can be calculated as follows [Ref.21]:

$$\sigma_t = \frac{2\rho_2 c_2}{\rho_2 c_2 + \rho_1 c_1}\sigma_o \qquad \text{(G.2)}$$

$$\sigma_r = \frac{\rho_2 c_2 - \rho_1 c_1}{\rho_2 c_2 + \rho_1 c_1}\sigma_o \qquad \text{(G.3)}$$

where subscripts "1" and "2" are used to indicate materials 1 and 2, respectively, and subcript "o" is used to indicate the original value of force.

It can be seen by utilization of Equation G.2 that an interface between two materials can dissipate a shock wave if the impedence of the second material is less than that of the first material. Likewise, the reflected shock will increase under the same conditions.

In this analysis, the two materials varied in the shank's base and top were steel and aluminum. Steel has a characteristic impedence of approximately 164 lb sec/in^3 [Ref. 21] while aluminum has a characteristic impedence of only 59.6 lb sec/in^3 [Ref. 21]. Therefore, it was expected that the steel base would transmit less and reflect more stress than the aluminum. This was found to be the case for our model.

LIST OF REFERENCES

1. Office of International Security and Peacekeeping Operations, *Hidden Killers: The Global Landmine Crisis*, US State Dept (1994).
2. Jane's Information Group, *Jane's Military Logistics and Vehicles* (1995).
3. Kinney, Gilbert F and Graham, Kenneth J , *Explosive Shocks in Air*, 2nd Edition, Springer-Verlag (1985).
4. ASTM, *Annual Book of ASTM Standards*, American Society for Testing and Materials, Philadelphia, Pa. Vol. 00.01 (1996).
5. D412-92, *Annual Book of ASTM Standards*, American Society for Testing and Materials, "Standard Test Methods for Vulcanized Rubber and Thermoplastic Rubbers and Thermoplastic Elastomers-Tension," Philadelphia, Pa. Vol. 09.01 (1996).
6. Brown, RP, *Physical Testing of Rubber*, 3rd Edition, Chapman and Hall, London (1996).
7. D575-91, *Annual Book of ASTM Standards*, American Society for Testing and Materials, "Standard Test Methods for Rubber Properties in Compression," Philadelphia, Pa. Vol. 09.01 (1996).
8. ASTM E8-96, *Annual Book of ASTM Standards*, American Society for Testing and Materials, "Standard Test Methods for Tension Testing of Metallic Materials," Philadelphia, Pa. Vol. 03.01 (1996).

9. D3039/D3039-95a, *Annual Book of ASTM Standards*, American Society for Testing and Materials, "Standard Test Method for Tensile Properties of Polymer Matrix Composites Materials," Philadelphia, Pa. Vol. 15.03 (1996).

10. Gibson, Ronald F., *Principles of Composite Material Mechanics*, McGraw-Hill, Inc., New York, (1994).

11. Brick, R.M. and Phillips, Arthur, *Structure and Properties of Alloys*, McGraw-Hill Book Company, Inc., New York (1949).

12. Uguaral, Ansel C. and Fenster, Saul K., *Advanced Strength and Applied Elasticity*, 3rd Edition, Prentice Hall, Upper Saddle River, NJ (1995).

13. Flinn, Richard A. and Trojan, Paul K., *Engineering Materials and Their Applications*, Houghton Mifflin Company, Boston, Ma (1981).

14. Peckner, Donald, *Handbook of Stainless Steels*, McGraw-Hill Book Co, New York (1977).

15. Agard, "Anthropomorphic Dummies for Crash and Escape Testing. Agard AR30" Advisory Group for Aerospace Research and Development, 1996.

16. Nahum, Alan M., and Melvin, John W, *Accidental Injury*, Springer-Verlag, New York (1993).

17. Woodfin, R.L., *Rigid Polyurethane Foam Technology for Countermine Program Phase 1*, Sandia National Laboratories, Albequerque, NM (1996).

18. ASTM E986-92, *Annual Book of ASTM Standards*, American Society for Testing and Materials, "Standard Practice for Scanning Electron Microscope Performance Characterization," Philadelphia, Pa. Vol. 03.01 (1996).

19. E-1508-93a, *Annual Book of ASTM Standards*, American Society for Testing and Materials, "Standard Guide for Quantitative Analysis by Energy-Dispersive Spectroscopy," Philadelphia, Pa. Vol. 03.01 (1996).

20. Gray, Allen G., *Source Book on Stainless Steel*, The Periodicals Publication Department, American Society for Metals, Metals Park, Ohio (1977).

21. Fujinaka, E.S., and MacDonald, J.L., *Research and Development of Protective Footwear*, Natick Laboratories, Natick, MA (1964).

INITIAL DISTRIBUTION LIST

No. of Copies

1. Defense Technical Information Center.....2
   8725 John J. Kingman Rd., Ste 0944
   Ft. Belvoir, VA 22060-6218

2. Dudley Knox Library.....2
   Naval Postgraduate School
   411 Dyer Rd.
   Monterey, CA 93943-5101

3. Professor Young W. Kwon, Code ME/Kw.....2
   Naval Postgraduate School
   411 Dyer Rd.
   Monterey, CA 93943-5101

4. Professor Young W. Kwon, Code ME/Mc.....2
   Naval Postgraduate School
   411 Dyer Rd.
   Monterey, CA 93943-5101

5. CPT Richard C. Muschek.....2
   P.O. Box 311904
   Enterprise, AL 36331-1904